

Geosphere

Paleoseismic history of the Fallen Leaf segment of the West Tahoe–Dollar Point fault reconstructed from slide deposits in the Lake Tahoe Basin, California-Nevada

Jillian M. Maloney, Paula J. Noble, Neal W. Driscoll, Graham M. Kent, Shane B. Smith, Gretchen C. Schmauder, Jeffrey M. Babcock, Robert L. Baskin, Robert Karlin, Annie M. Kell, Gordon G. Seitz, Susan Zimmerman and John A. Kleppe

Geosphere published online 26 June 2013;
doi: 10.1130/GES00877.1

- Email alerting services** click www.gsapubs.org/cgi/alerts to receive free e-mail alerts when new articles cite this article
- Subscribe** click www.gsapubs.org/subscriptions/ to subscribe to Geosphere
- Permission request** click <http://www.geosociety.org/pubs/copyrt.htm#gsa> to contact GSA

Copyright not claimed on content prepared wholly by U.S. government employees within scope of their employment. Individual scientists are hereby granted permission, without fees or further requests to GSA, to use a single figure, a single table, and/or a brief paragraph of text in subsequent works and to make unlimited copies of items in GSA's journals for noncommercial use in classrooms to further education and science. This file may not be posted to any Web site, but authors may post the abstracts only of their articles on their own or their organization's Web site providing the posting includes a reference to the article's full citation. GSA provides this and other forums for the presentation of diverse opinions and positions by scientists worldwide, regardless of their race, citizenship, gender, religion, or political viewpoint. Opinions presented in this publication do not reflect official positions of the Society.

Notes

Advance online articles have been peer reviewed and accepted for publication but have not yet appeared in the paper journal (edited, typeset versions may be posted when available prior to final publication). Advance online articles are citable and establish publication priority; they are indexed by GeoRef from initial publication. Citations to Advance online articles must include the digital object identifier (DOIs) and date of initial publication.

Paleoseismic history of the Fallen Leaf segment of the West Tahoe–Dollar Point fault reconstructed from slide deposits in the Lake Tahoe Basin, California–Nevada

Jillian M. Maloney¹, Paula J. Noble², Neal W. Driscoll¹, Graham M. Kent³, Shane B. Smith², Gretchen C. Schmauder³, Jeffrey M. Babcock¹, Robert L. Baskin⁴, Robert Karlin², Annie M. Kell³, Gordon G. Seitz⁵, Susan Zimmerman⁶, and John A. Kleppe⁷

¹*Scripps Institution of Oceanography, University of California, San Diego, 9500 Gilman Drive, La Jolla, California 92093, USA*

²*Department of Geological Sciences & Engineering, University of Nevada, Reno, Nevada 89557-0138, USA*

³*Nevada Seismological Laboratory, University of Nevada, Reno, Nevada 89557-0174, USA*

⁴*U.S. Geological Survey, West Valley City, Utah 84119, USA*

⁵*California Geological Survey, 345 Middlefield Road, MS 520, Menlo Park, California 94025, USA*

⁶*Center for Accelerator Mass Spectrometry, Lawrence Livermore National Laboratory, Livermore, California 94550, USA*

⁷*College of Engineering, University of Nevada, Reno, Nevada 89557-0256, USA*

ABSTRACT

The West Tahoe–Dollar Point fault (WTDPF) extends along the western margin of the Lake Tahoe Basin (northern Sierra Nevada, western United States) and is characterized as its most hazardous fault. Fallen Leaf Lake, Cascade Lake, and Emerald Bay are three subbasins of the Lake Tahoe Basin, located south of Lake Tahoe, and provide an opportunity to image primary earthquake deformation along the WTDPF and associated landslide deposits. Here we present results from high-resolution seismic Chirp (compressed high intensity radar pulse) surveys in Fallen Leaf Lake and Cascade Lake, multibeam bathymetry coverage of Fallen Leaf Lake, onshore Lidar (light detection and ranging) data for the southern Lake Tahoe Basin, and radiocarbon dates from piston cores in Fallen Leaf Lake and Emerald Bay. Slide deposits imaged beneath Fallen Leaf Lake appear to be synchronous with slides in Lake Tahoe, Emerald Bay, and Cascade Lake. The temporal correlation of slides between multiple basins suggests triggering by earthquakes on the WTDPF system. If this correlation is correct, we postulate a recurrence interval of ~3–4 k.y. for large earthquakes on the Fallen Leaf Lake segment of the WTDPF, and the time since the most recent event (~4.5 k.y. ago) exceeds this recurrence time. In addition, Chirp data

beneath Cascade Lake image strands of the WTDPF offsetting the lake floor as much as ~7.5 m. The Cascade Lake data combined with onshore Lidar allow us to map the WTDPF continuously between Fallen Leaf Lake and Cascade Lake. This improved mapping of the WTDPF reveals the fault geometry and architecture south of Lake Tahoe and improves the geohazard assessment of the region.

INTRODUCTION

Onshore and offshore research in the Lake Tahoe Basin (northern Sierra Nevada, western United States) has defined the geometry and slip rates of the major faults accommodating active extension across the basin (Brothers et al., 2009; Dingler et al., 2009; Gardner et al., 2000; Karlin et al., 2005; Kent et al., 2005; Schweickert et al., 2004; Seitz et al., 2006, 2005). These faults, the Stataline–North Tahoe fault, Incline Village fault, and the West Tahoe–Dollar Point fault (WTDPF), exhibit down to the east normal displacement (Dingler et al., 2009) (Fig. 1A). Recent work in Fallen Leaf Lake has helped identify the WTDPF as potentially the most hazardous fault in the Lake Tahoe Basin, with the potential to produce $M > 7.0$ earthquakes (Brothers et al., 2009). The WTDPF is a major north-south–striking normal fault, extending >50 km along the western margin of the Lake Tahoe Basin, and is divided by geomorphic disconti-

nities into three main segments: the southern Fallen Leaf Lake segment, central Rubicon segment, and northern Dollar Point segment (Fig. 1A). The most recent event (MRE) on the Fallen Leaf Lake segment was 4.57–4.85 k.y. ago. The MRE on the Rubicon segment was dated as ca. 5.3–5.6 ka (Smith et al., 2013). A recurrence interval for the WTDPF of ~4.8 k.y. was estimated by Kent et al. (2005) based on slip-rate models, but the paleoseismic record has not been extended past the MREs on the Fallen Leaf Lake and Rubicon segments. Furthermore, rupture timing patterns between the three WTDPF segments, Incline Village fault, and Stataline–North Tahoe fault remain poorly understood.

Historic earthquakes have been shown to trigger mass movements in lacustrine and marine environments (Hampton et al., 1996; Lee et al., 2009); recent studies have used slide deposits observed in sediment cores and seismic reflection data to estimate earthquake recurrence intervals (Goldfinger et al., 2007; Schnellmann et al., 2002; Strasser et al., 2006; Upton and Osterberg, 2007). Several lines of evidence argue for seismic triggering of slide deposits, but the most convincing is a record of synchronous deposits across broad areas and multiple basins. Compressed high intensity radar pulse (Chirp) data beneath the Lake Tahoe subbasins Fallen Leaf Lake, Cascade Lake, and Emerald Bay image several large slide deposits correlated temporally between the three subbasins, as well as with previously dated slides in Lake

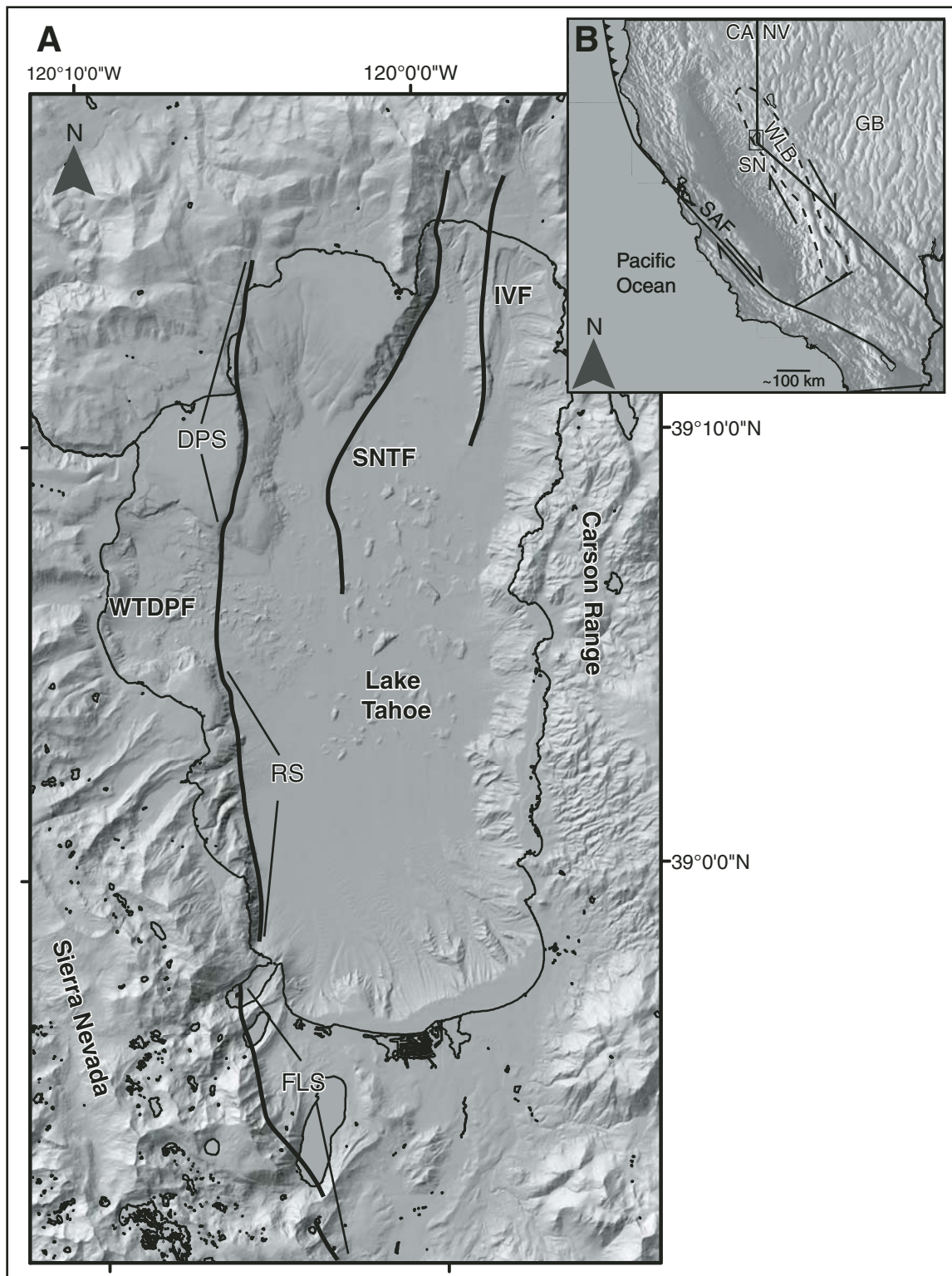


Figure 1. (A) Map of the Lake Tahoe Basin and surrounding area showing generalized fault traces of the West Tahoe–Dollar Point fault (WTDPF), Stateline–North Tahoe fault (SNTF), and Incline Village fault (IVF). Three segments of the WTDPF are also labeled: the northern Dollar Point segment (DPS), central Rubicon segment (RS), and southern Fallen Leaf segment (FLS) (modified from Brothers et al., 2009). (B) Regional plate boundary map showing location of the San Andreas fault (SAF), Walker Lane Belt (WLB), Sierra Nevada Range (SN), and the Great Basin (GB). The Lake Tahoe Basin is located within the northwestern WLB, on the border between California (CA) and Nevada (NV).

Paleoseismic history of the Fallen Leaf segment of the West Tahoe–Dollar Point fault

Tahoe (Smith et al., 2013). Based on extent and timing, we suggest that four of the slides were triggered by events on the WTDPF; if correct, these coseismic slides extend the paleoseismic record for the WTDPF and provide new insights into the rupture patterns along strike, and possibly between faults. Examination of the extended paleoseismic record yields a recurrence interval of ~3–4 k.y. on the Fallen Leaf Lake segment of the WTDPF; this is vital in assessing geohazards posed by the WTDPF to the populated Lake Tahoe Basin.

BACKGROUND

The Lake Tahoe Basin is located in the northern Walker Lane deformation belt, and is the westernmost basin in a series of north-south-trending basins and mountain ranges bounded by normal faults (Faulds et al., 2005; Unruh et al., 2003). The Walker Lane is located between the Sierra Nevada block and the central Great Basin, and is characterized by trans-tensional deformation caused by the oblique divergence of the Sierra Nevada–Central Valley microplate and stable North America (Fig. 1B) (Argus and Gordon, 2001; Oldow, 2003; Unruh et al., 2003). Geodetic studies indicate 9–13 mm/yr of dextral shear in the Walker Lane deformation belt, which amounts to ~20%–25% of the total plate motion between the North American and Pacific plates (Bennett et al., 2003; Dixon et al., 2000; Hammond and Thatcher, 2004; Svarc et al., 2002).

The Lake Tahoe Basin is an asymmetric half-graben set between the Sierra Nevada and Carson mountain ranges, and has been tectonically active for at least 3 m.y. (Dingler et al., 2009; Faulds et al., 2005; Hyne et al., 1972; Kent et al., 2005; Schweickert et al., 2004; Surpless et al., 2002). Extension across the basin is accommodated by three primary normal fault systems: the WTDPF, Stateline–North Tahoe fault, and Incline Village fault (Kent et al., 2005), which have vertical slip rates of 0.4–0.8 mm/yr, 0.35–0.6 mm/yr, and 0.18–0.30 mm/yr, respectively (Brothers et al., 2009; Dingler et al., 2009).

Fallen Leaf Lake, Cascade Lake, and Emerald Bay are bounded by lateral Tioga (ca. 30–14 ka; Benson et al., 1998; Bischoff and Cummins, 2001; Clark and Gillespie, 1997; Howle et al., 2012; Phillips et al., 1996; Rood et al., 2011) and Tahoe glacial moraines on their eastern and western shores (Saucedo et al., 2005). Fallen Leaf Lake and Cascade Lake are separated from Lake Tahoe by recessional end moraines, whereas Emerald Bay connects with Lake Tahoe to the north at Emerald Point. Input of modern sediment to Fallen Leaf Lake is sourced mainly from Glen Alpine Creek, which drains an area

of ~42 km² from the Desolation Wilderness to the south. Additional input to the lake is sourced from Cathedral Creek and several unnamed creeks along the western shore that drain from the mountains to the southwest. Sediment input to Cascade Lake is mainly from Cascade Creek, which drains an area of ~12 km². Input to Emerald Bay is mainly from Eagle Creek, which drains an area of ~25 km² from the mountains to the southwest. Granitic rocks of the Sierra Nevada batholith and metamorphosed roof pendants characterize the geology of the drainage areas for all three subbasins (Saucedo et al., 2005). Several Pleistocene–Holocene landslide deposits have been mapped onshore near the subbasins (Saucedo et al., 2005). Slides are mapped above the southernmost shores of both Emerald Bay and Cascade Lake and appear to spill into the basins very near the WTDPF (Fig. 2). Two slides are also mapped slightly northwest from Cathedral Creek, above Fallen Leaf Lake.

Debris flow and turbidite deposits have been identified in cores and seismic reflection data in Lake Tahoe sediments, and seismic triggering of the deposits has been suggested (Dingler et al., 2009; Karlin et al., 2005; Kent et al., 2005; Seitz et al., 2006; Smith et al., 2013). Smith et al. (2013) mapped and dated 18 debris flow and turbidite deposits in Lake Tahoe, 4 of which appear to be triggered by events on the Lake Tahoe Basin faults. Three events were triggered by events on the WTDPF: deposit F (4.51–4.07 ka), deposit G (5.60–5.33 ka), and deposit J (7.89–7.19 ka). Several deposits younger than deposit J were also linked to events on faults outside the Lake Tahoe Basin. Older event deposits were also identified and dated as deposits K (9.45–8.77 ka), L (9.73–9.32 ka), M (10.16–9.80 ka), N (11.26–10.48 ka), and O (12.49–11.20 ka), but the triggering earthquake events for these deposits are poorly constrained, and in some cases may be related to motion on the Stateline–North Tahoe fault.

METHODS

Fallen Leaf Lake bathymetric data were collected in July 2010 using a Reson 7125 multi-beam system operated at 200 kHz (Fig. 3) with a nominal vertical resolution of ~2.5 cm. Positions were calculated through a dual-differential global positioning system (GPS) system, providing lateral position accuracy to better than 2 m. Data were processed using Caris HIPS and SIPS software (<http://www.caris.com/products/hips-sips/>), and interpreted with QPS Fledermaus and ArcGIS (<http://www.qps.nl/display/fledermaus/main>; www.esri.com) software packages. The U.S. Geological Survey (USGS) Fallen Leaf Lake water-level datum of 1944 m

(North American Vertical Datum, NAVD88) was used to correlate with onshore Lidar (light detection and ranging) data.

In June 2011, ~45 line km of Chirp seismic data were acquired from Fallen Leaf Lake and Cascade Lake (Figs. 2B, 2C). The Chirp profiler was operated with a 30 ms swept pulse of 1–15 kHz, and provided decimeter vertical resolution and subbottom penetration >50 m. Location accuracy is to within 5 m. Data were processed using SIOSEIS (Henkart, 2003) software and imported to Kingdom Suite (<http://www.ih.com/>) and QPS Fledermaus software packages for interpretation. A nominal water and sediment velocity of 1450 m/s was assumed for all depth and sediment thickness conversions.

Piston cores from four locations were acquired in Fallen Leaf Lake during November 2010 using a Kullenberg piston coring system from LaCore (University of Minnesota; Fig. 2C). Core BC1A, taken near the basin depocenter, is 9.8 m long and penetrated the entire Holocene package into the Pleistocene periglacial deposits below. The piston cores were logged for lithology, magnetic susceptibility, and sampled for micropaleontology, geochemistry, and radiocarbon dating (Karlin et al., 2011). Plant macrofossils were extracted from the cores for radiocarbon dating and submitted to the Lawrence Livermore National Laboratory Center for Accelerator Mass Spectrometry (CAMS). Calibrated radiocarbon ages were determined using OxCal v. 4.1.7 (Bronk Ramsey, 2009) with the IntCal 04 calibration curve (Reimer et al., 2004) (Table 1). The ages of the two youngest event deposits in Fallen Leaf Lake were modeled as a sequence in OxCal v. 4.1.7 using bounding dates from three cores taken in 2010 and a core taken in 2006 (PC3; Brothers et al., 2009). Older event deposit ages were calculated based on the overall age model for core BC1A (Karlin et al., 2011) (Table 1). We observe a systematic offset of ~0.5 m between core depth and Chirp depth calculated using a nominal 1450 m/s velocity.

A previously collected piston core (EB2) from Emerald Bay (Dingler et al., 2009) was used to calculate ages for event deposits observed in Emerald Bay Chirp data. Three macrofossil samples were analyzed at the CAMS Laboratory and calibrated radiocarbon ages were determined using OxCal v. 4.1.7 (Bronk Ramsey, 2009) and the IntCal 04 calibration curve (Reimer et al., 2004; Table 1).

RESULTS**Fallen Leaf Lake Bathymetry**

The maximum depth of Fallen Leaf Lake as recorded in multibeam data is ~116 m below

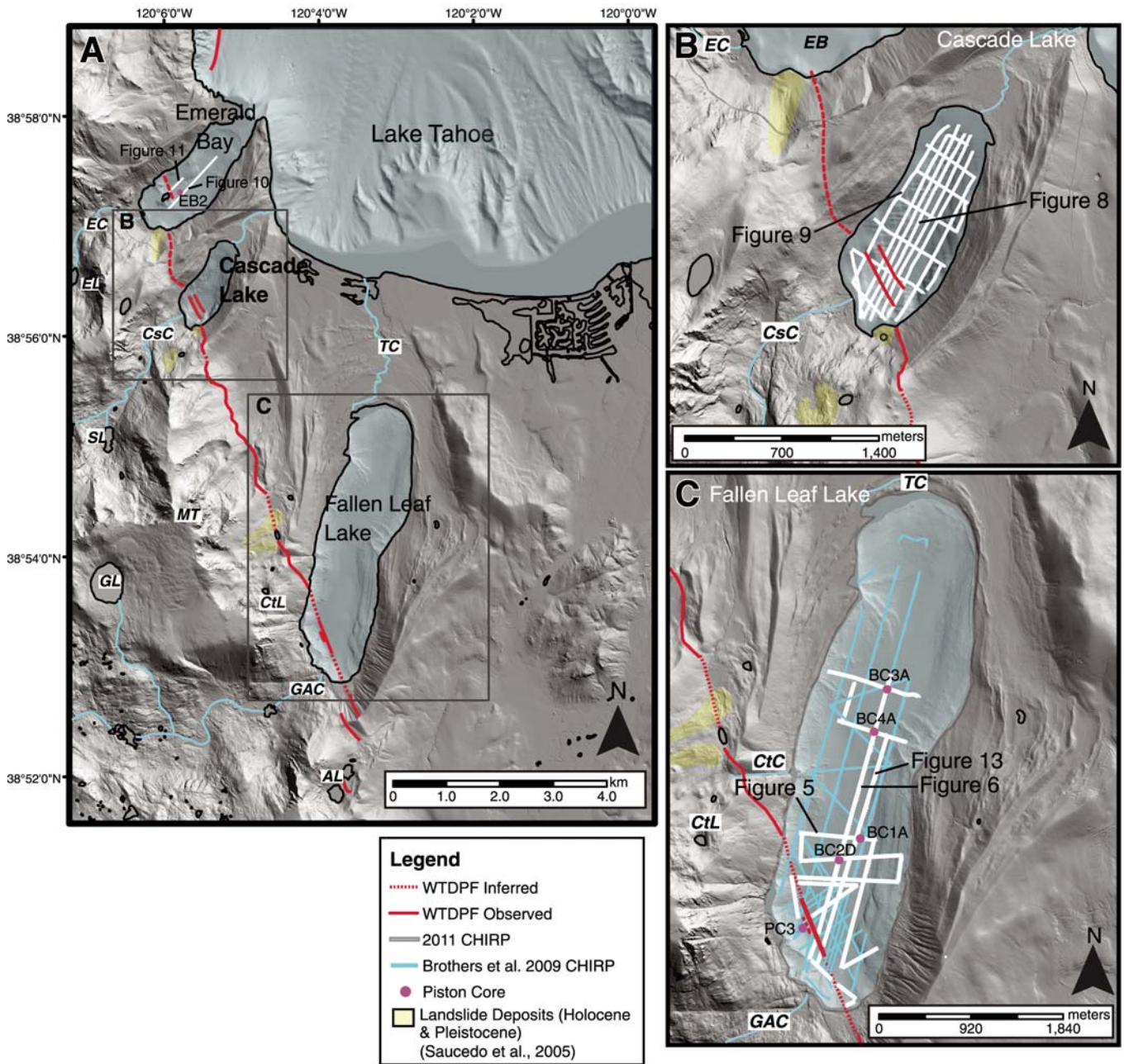


Figure 2. (A) Map of the southern Lake Tahoe Basin including the subbasins Emerald Bay (EB), Cascade Lake, and Fallen Leaf Lake. Bathymetry of Lake Tahoe and Emerald Bay is from Gardner et al. (2000) retrieved from U.S. Geological Survey (2001). Trace of the West Tahoe–Dollar Point fault (WTDPF) beneath Lake Tahoe is from Brothers et al. (2009) and Dingler et al. (2009). Onshore topography is from aerial Lidar (light detection and ranging) surveys (Tahoe Regional Planning Agency, 2010). Bathymetry and topography are 1 m grids shaded from an azimuth of 315° and elevation of 45°. CHIRP—compressed high intensity radar pulse. (B) Enlargement of Cascade Lake area. (C) Enlargement of Fallen Leaf Lake area. See inset legend for further details. Abbreviations: AL—Angora Lakes, CsC—Cascade Creek, CtL—Cathedral Lake, CtC—Cathedral Creek, EL—Eagle Lake, EC—Eagle Creek, GL—Gilmore Lake, GAC—Glenn Alpine Creek, MT—Mount Tallac, SL—Snow Lake, TC—Taylor Creek.

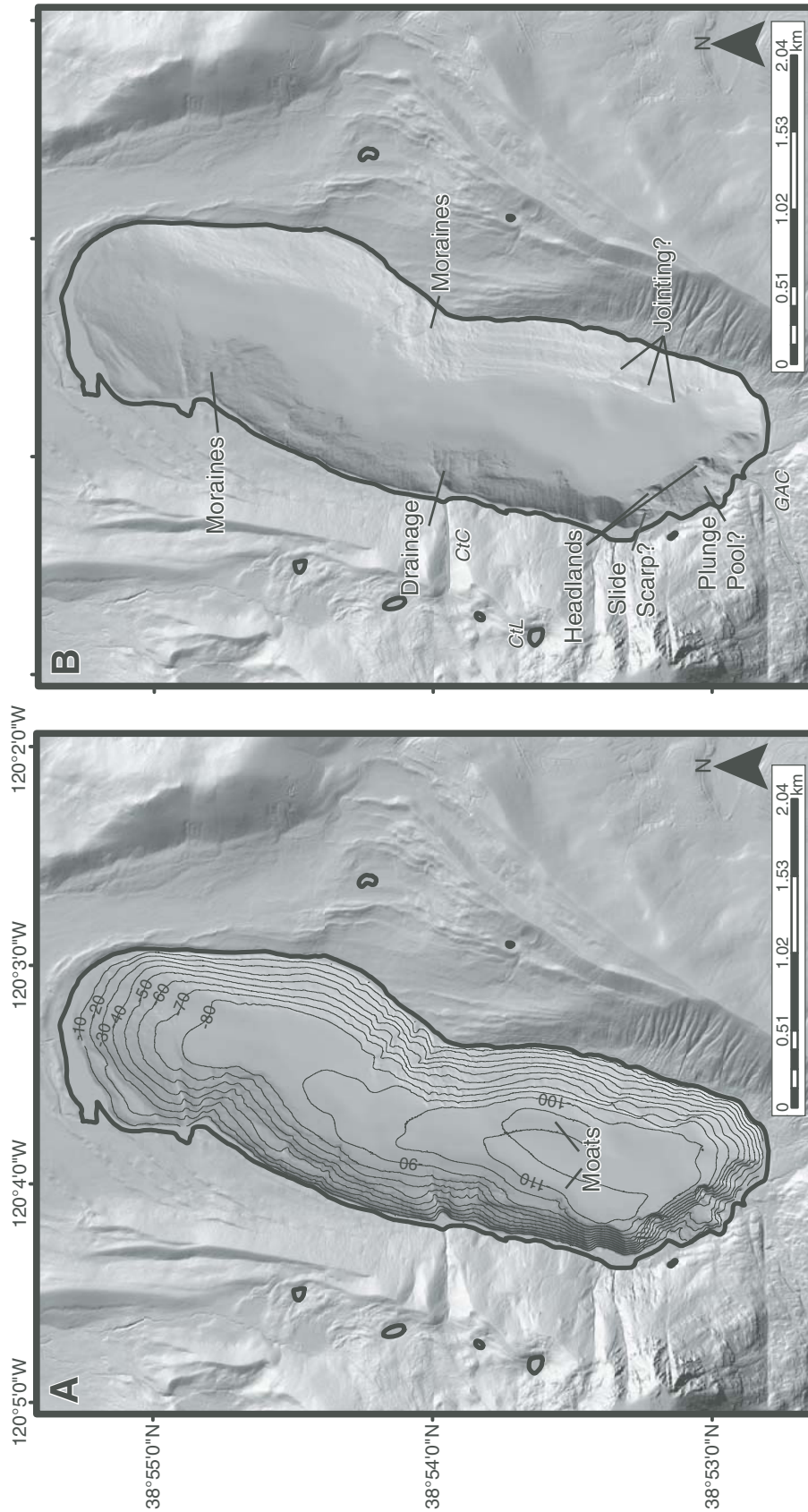


Figure 3. (A) Hillshaded bathymetry of Fallen Leaf Lake from the 2010 multibeam survey with 10 m contours from -10 m to -110 m. Depths are below the U.S. Geological Survey 1944 m lake level. Solid gray areas between the bathymetry and lakeshore are areas of no data. (B) Hillshaded bathymetry without contours to highlight lake floor features. Also shown are Cathedral Creek (CtC) and Glen Alpine Creek (GAC) inputs to the lake. CtL—Cathedral Lake. Labeled features are described in detail in the text. For both figures, the topography is from aerial Lidar (light detection and ranging) surveys. Bathymetry and topography are 1 m grids shaded from an azimuth of 315° and elevation of 45°.

TABLE 1. RADIOCARBON AGES FOR FALLEN LEAF LAKE AND EMERALD BAY CORES

Location	Sample name	Lab sample*	Depth (m) [†]	$\delta^{13}\text{C}$ [‡]	Uncalibrated ¹⁴ C age (yr B.P.)	Calibrated calendar age [#]	Confidence (%)	Rounded age (ky ago)**
Core BC1A (FLL)	Bolly-1A3-65	152695	2.285	-25	3735 ± 30	4155-3963 4221-4208	93.4	4.0-4.2
	Bolly-1A5-22	152542	4.105	-25	4515 ± 45	5313-5039 4996-4983	94.1	5.0-5.3
	Bolly-1A5-142	152696	5.290	-25	6165 ± 30	7164-6975 9032-8768	95.4	7.0-7.2
	Bolly-1A6-149	152543	6.860	-25	8045 ± 40	9076-9062	94.5	8.8-9.1
	Bolly-1A7-5.5	152544	6.935	-25	8190 ± 45	9279-9020	95.4	9.0-9.3
	Bolly-1A8-55	152545	8.940	-25	10335 ± 35	12251-12037 12380-12260	71.5	12.0-12.4
Core BC2D (FLL)	Bolly-2D3-46	152688	3.230	-25	4120 ± 30	4726-4527 4815-4753	70.4	4.5-4.8
	Bolly-2D4-28	152689	4.410	-25	4630 ± 40	5471-5291 5570-5559	25.0	5.3-5.6
	Bolly-2D6-77.5	152702	6.725	-25	6805 ± 35	7687-7586 8778-8592	95.4	7.6-7.7
	Bolly-2D8-7.5	152703	8.385	-25	7885 ± 30	8860-8834	92.0	8.6-8.9
						8933-8922	2.4	
						8946-8944	0.8	
Core BC3A (FLL)	Bolly-2D-734 ^{††}		6.875		7015 ± 45	7946-7739	0.2	7.7-7.9
	Bolly-3A1-105.5	152707	1.040	-25	2750 ± 35	2928-2767	95.4	2.8-2.9
	Bolly-3A2-66	152709	2.185	-25	4980 ± 45	5763-5604 5889-5809	77.1	5.6-5.9
	Bolly-3A3-18.25	152710	3.250	-25	6640 ± 35	7580-7460	18.3	7.5-7.6
	FLL-PC3-110	152721	1.100	-25	3670 ± 30	4088-3905	95.4	3.9-4.1
	FLL-PC3-383 ^{§§}	AA76374	3.830	-25.6	4235 ± 44	4765-4620 4869-4785	49.8	4.6-4.9
Core EB2 (EB)	EB2-1	94940	0.880	-25	1995 ± 40	2056-1865 1841-1837	95.1	1.8-2.1
	EB2-2	94941	3.765	-25	4280 ± 40	4967-4815 4754-4711	0.3	4.7-5.0
	EB2-3	94942	4.260	-25	4610 ± 70	5480-5211 5199-5048	5.6	5.0-5.6
					5578-5534	67.5		
						23.5		
						4.3		

Note: FLL—Fallen Leaf Lake; EB—Emerald Bay.

*Sample analysis was performed at the Center for Accelerator Mass Spectrometry at Lawrence Livermore National Laboratory, with the exception of FLL-PC3-383, which was analyzed at the University of Arizona Accelerator Mass Spectrometry Laboratory.

[†]Measured from top of core.

[‡] $\delta^{13}\text{C}$ values of -25 were not measured, but are the assumed values according to Stuiver and Polach (1977).

[#]Calibrated ages determined using OxCal version 4.1.7 (Bronk Ramsey, 2009) and IntCal04 atmospheric curve (Reimer et al., 2004). Calibrated ages are reported as yr ago % confidence under the 95% probability distribution. The highest probability calibrated range for each date is shown in bold italics.

**Rounded to nearest 0.1 ky.

^{††}Tsuyowata Ash age from Bacon (1983).

^{§§}Data from Brothers et al. (2009).

the USGS datum at 1944 m elevation (Fig. 3). Steep slopes bound the basin on the southern, eastern, and western shorelines ($\sim 15^{\circ}$ – 40°), with a more gently dipping slope to the north ($< 10^{\circ}$). Several prominent features with high slope and rugosity are observed along the basin slopes. The steep basin slopes change abruptly at the basin floor, which is gently sloping with low rugosity. The deepest areas of the basin are represented by two moats that extend along the base of the eastern and western slopes in the southern basin. The moats encircle a subparallel mound. There are other smaller mounds and depressions on the basin floor, but regionally it slopes gently up to the north.

The expression of the WTDPF is observed on the basin floor as a linear depression that trends $\sim N20^{\circ}W$. A second splay may also occur along the base of the steeply sloping southern wall. These expressions of the fault on the lake floor align well with traces of the WTDPF splays mapped in Chirp data.

Along the basin slopes, several ridges, interpreted as recessional moraines, extend from the shore to the basin floor. Three prominent ridges are located near the center of the eastern slope and three additional ridges are located along the northwestern slope. The crests range in height between ~ 1 and 15 m. Several less prominent ridges are located along the western slope. A fan-shaped ridge feature on the eastern slope is offshore the mouth of Cathedral Creek.

Three prominent parallel scarps are located near the base of the eastern slope. The scarps are evenly spaced ~ 220 m apart, trend $\sim N20^{\circ}W$, and each exhibits ~ 10 m of down to the southwest vertical offset of the lake floor at the basinward edge. In Chirp data, we observe a topographic high in the acoustic basement adjacent to these features, but we do not observe evidence for associated faulting of basin sediments, and therefore do not interpret them to be faults.

Along the southern slope, two small headland features slope steeply to the basin floor. Above the southeastern headland is a circular, flat area at ~ 40 m water depth. Shoreward to the southeast, the plateau is bounded by steeply dipping slopes leading up to the modern shoreline. Shoreward to the northeast a more gently sloping ramp leads up to the shore. The ramp is bordered on the basinward edge by a ridge trending $S55^{\circ}E$. The ridge crest is highest (~ 5 m) near-shore, and decreases as it wraps around the edge of the plateau (~ 1 m). The ridge ends where it meets the southeastern headland on the slope to the basin floor. The mouth of Glen Alpine Creek empties just to the southeast of the plateau and headland. A small debris fan is adjacent to the northwestern headland and spills slightly out onto the basin floor. Above this fan there are

three scarps oriented $\sim N5^{\circ}W$. The scarps are ~ 10 – 15 m high.

Seismic Stratigraphy

Fallen Leaf Lake

Based on acoustic character, we divide Fallen Leaf Lake sediments into two major groups, section I and section II, and one minor group, section III. Section I is further subdivided into units A, B, and C (e.g., Brothers et al., 2009). Section III infills topographic lows in the northern basin and is not observed basin wide. Sub-horizontal, parallel reflectors characterize section II; in contrast, section I exhibits a distinct lenticular geometry.

We describe the sequences from oldest to youngest. The acoustic basement is the basal layer imaged by Chirp data and the relief on this surface is shown in Figure 4. Little to no lacustrine sediment is observed on the steep basin walls. The depth to basement is greatest in the southern basin and shoals to the north. In the deepest areas, acoustic basement is not visible in the Chirp profiles, and thus the depth to

basement is a minimum estimate (Fig. 4). The acoustic basement is hummocky throughout the basin; several mounds and ridges form complex topography. A large topographic high in the acoustic basement is located adjacent to prominent modern scarps observed on the southeast basin slope in bathymetry data (Figs. 3 and 4). The central basin trends north in a tortuous path and is interrupted by several features. A large mound at the center of the basin has a long axis that extends roughly north-south and its height tapers to the north (Figs. 4 and 5). Other topographic highs in the northern basin form ridges that extend across the basin trending roughly northwest-southeast. The ridges observed in the acoustic basement relief map (Fig. 4) occur near the bathymetric ridges mapped along the eastern slope (Fig. 3). These features divide the basin into a southern and northern zone, and are referred to herein as mid-lake moraines (Figs. 4 and 6). The southern zone is a deep basin with steeply sloping walls and isolated topographic highs. The northern zone is shallower, with more gently sloping walls and highly variable topography in the acoustic basement (Fig. 4).

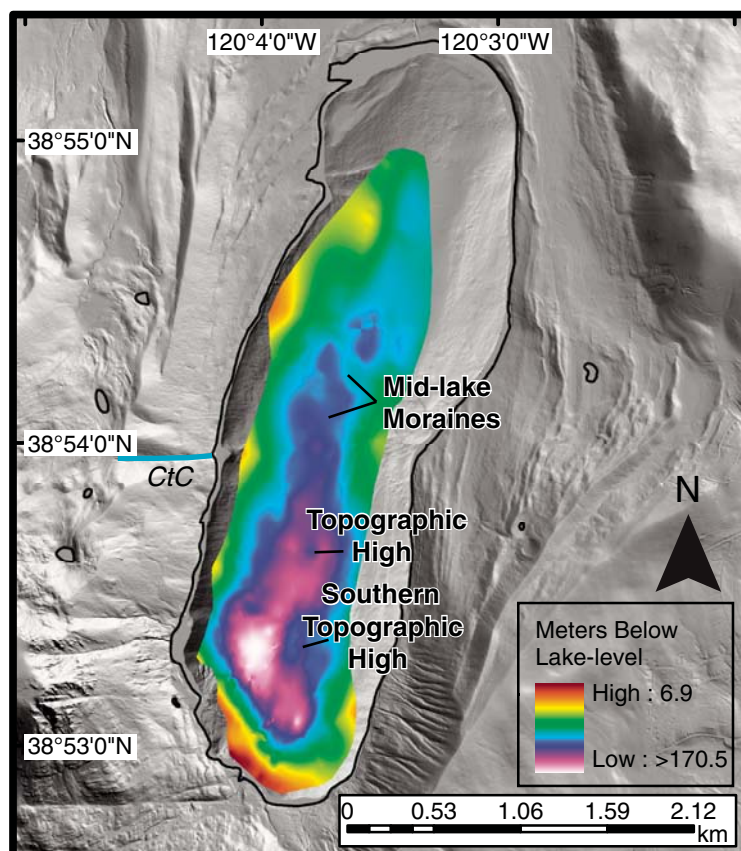


Figure 4. Topography of the acoustic basement traced in, and gridded between, Chirp (compressed high intensity radar pulse) profiles. Labeled features are discussed in the text. CtC—Cathedral Creek.

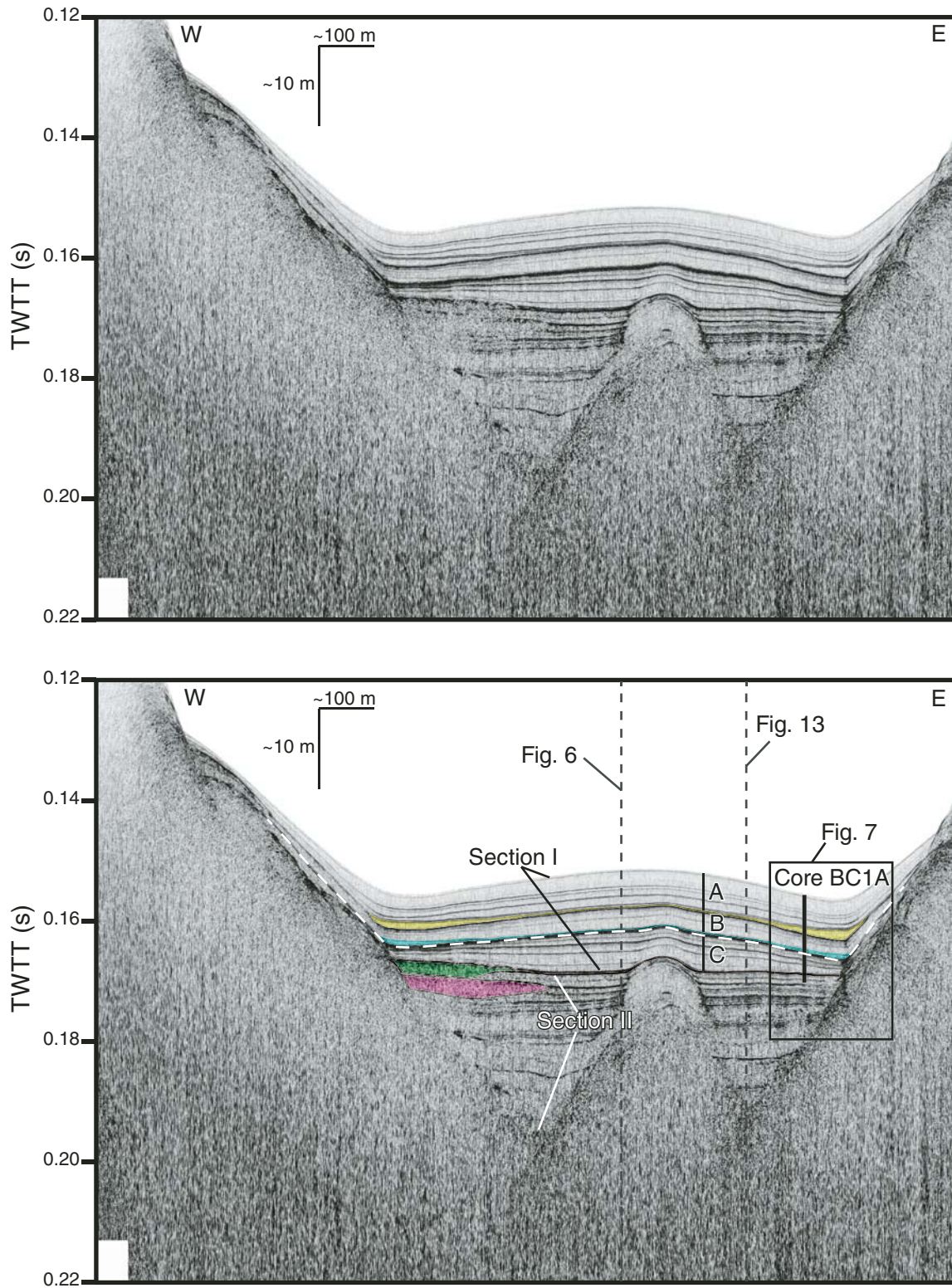


Figure 5. East-west Chirp (compressed high intensity radar pulse) profile showing Fallen Leaf Lake slides FLLS1 (yellow), FLLS2 (blue), FLLS3 (green), and FLLS4 proximal slide (pink). This profile also illustrates the sedimentary packages defined in the text. Section II, section I, and units A, B, and C are labeled. The white dashed horizon represents the Tsoyowata Ash horizon. The enlargement near core BC1A is shown in Figure 7. TWTT—two-way traveltime.

Paleoseismic history of the Fallen Leaf segment of the West Tahoe–Dollar Point fault

The shape of the acoustic basement in these two zones appears to control sediment dispersal and results in differential deposition between the northern and southern zones.

Section III is observed between the acoustic basement and section I north of the mid-lake moraines. This package is chaotic, with some wavy, high-amplitude, discontinuous reflectors (Fig. 6). The package infills topographic lows and thins onto highs in the acoustic basement topography of the northern basin, particularly around the mid-lake moraine complex. The upper contact of section III is wavy and in some locations hummocky. Generally the unit is more chaotic near the base and systematically exhibits more acoustic reflectors toward the upper contact. There is a marked contrast between section III and the more transparent units of section I above. Section III was beyond the penetration depth for all sediment cores.

Section II is only observed in the southern zone of the basin and has a maximum thickness of >40 m. The section consists of parallel continuous reflectors separating semitransparent layers of varying thickness (Figs. 5 and 6). Both high- and low-amplitude reflectors are observed within section II; there is a large thickness variability between reflectors. The high-amplitude reflectors are vertically farther apart near the base of section II and become more numerous and closely spaced near the upper contact (ranging from ~1 m to several meter spacing). Where visible, the low-amplitude reflectors are very closely spaced (decimeter scale), and appear to be clustered. In the deepest part of the basin, the reflectors remain mostly horizontal, except where offset by the WTDPF. The contact of the reflectors and the steep basin walls is generally a straight, lateral onlap. To the north, reflectors of section II shoal, converge, and eventually onlap the acoustic basement as it slopes upward toward the mid-lake moraines (Fig. 6). The reflectors appear to maintain a constant amplitude signal throughout the southern basin.

The base of section II was identified as the acoustic basement where visible, but it was beyond the penetration depth of the Chirp in the deepest portions of the southern basin. Based on acoustic character, section II is not observed north of the mid-lake moraines. Nevertheless, we cannot rule out that there may be a highly condensed unit of section II that we grouped either with section III or section I. The upper contact of section III marks a change in stratal geometry from flat-lying beds below to lenticular shaped beds in section I above (Fig. 5). This contact was recovered in core BC1A at 8.5 m downcore, where it is marked by a thin turbidite laterally traceable to a slide deposit observed in

Chirp data (Fig. 7). The proximal expression of this slide is observed to the west in Chirp data at the upper contact of section II (Fig. 5). The upper contact of section II is placed directly below the turbidite. Lithologically, there is a change in sediment character below the turbidite where it transitions into a 0.6 m interval of laminated silty clay. Below the laminated interval is a thin layer of bluish clay, below which is 0.6 m of glacial silt. The upper contact of section II also marks a change in magnetic susceptibility, which is almost zero at the base of section I, and increases downward through the laminated interval and into the glacial silt unit below the bluish clay layer (Fig. 7). We calculate the age of the upper contact of section II to be ca. 11.24–11.64 ka (95% confidence level) based on our age model with a median age of 11.44 ka (Table 1; Fig. 7).

Section I is divided into three units, separated by slide deposits; units A and B are separated by the FLLS1 slide (FLL is Fallen Leaf Lake) and units B and C are separated by the FLLS2 slide (Fig. 5). The slide deposits are easily identified in Chirp data because they infill topographic lows associated with lenticular deposits that characterize section I (Fig. 5). These topographic lows form moats on the lake floor adjacent to the steep walls (Fig. 3). The slides preferentially infill the moats, obscuring in part their relief, and are used as marker beds for correlation to sediment cores (Fig. 7). The units of section I exhibit lateral variation in thickness across the basin. All three units were recovered in piston cores (Fig. 7). Unit C is characterized by olive and yellow clay with banding partially disturbed by bioturbation. Unit B is characterized by yellowish-olive clay with subtle banding and mottling. The lower section of unit A is similar in lithology to unit B, with an upper section characterized by homogeneous olive mud (Fig. 7). In many cases magnetic susceptibility spikes in the core correspond to high-amplitude reflections in Chirp data. Units A, B, and C exhibit similar acoustic character. Each unit consists of variable thickness transparent layers separated by thin, continuous reflectors of low to high amplitude. Unit C contains more high-amplitude reflectors than units A and B. To the north, the transparent packages for all units thin and the reflectors converge and decrease in amplitude (Fig. 6). Layers within units A, B, and C extend up the basin slopes and onlap the acoustic basement well above the lake floor (Fig. 5). In the southern basin, each unit exhibits a lenticular geometry that is thickest near the basin center and thins toward the eastern and western basin slopes (Fig. 5). In some profiles, the reflectors appear to be truncated by slide deposits (Fig.

5). The lenticular pattern does not extend to the northern basin; instead, the units in the northern basin thin toward highs in topography and are fairly uniform in thickness.

Cascade Lake

The acoustic character of stratigraphic packages in Cascade Lake is similar to that observed in Fallen Leaf Lake, and allows for a stratigraphic correlation between the two basins. The acoustic basement is hummocky, with steep slopes on the southern, eastern, and western sides and a gentler slope up to the north (Figs. 8 and 9). The deepest part of the basin is in the south, near the WTDPF. Based on acoustic character, the stratigraphy can be divided into three sections that have characteristics similar to those of sections I, II, and III in Fallen Leaf Lake (Fig. 8). The oldest sedimentary unit, section III, is chaotic and homogeneous with some discontinuous and wavy low- to high-amplitude reflectors that infill lows and thin onto basement highs. In the deepest area of the basin, the uppermost part of section III is represented by thinly spaced (decimeter scale), high-amplitude, wavy, and mostly continuous reflectors that separate semitransparent layers. The upper contact of section III is a high-amplitude reflector that separates the thinly spaced reflectors below from section II above. Continuous, subparallel, high-amplitude reflectors that separate semitransparent layers of variable thickness (approximately decimeter to meter scale) are characteristic of section II. These beds thin onto highs in topography, but do not extend north beyond the southern depocenter. The high-amplitude reflectors maintain a strong signal throughout the basin. Some thinly spaced (decimeter scale), low-amplitude reflectors are apparent within the semitransparent layers (Fig. 8). The uppermost package, section I, is divided into two units separated by the dashed line in Figure 8.

Semitransparent layers that are separated by high-amplitude reflectors characterize the lower unit. The reflectors become more closely spaced moving upsection. This unit was grouped with section I rather than section II because it drapes over highs in topography away from the southern depocenter, whereas section II onlaps topographic relief and is restricted to the southern depocenter. Within section I, the lower unit is separated from the upper unit by a high-amplitude reflector that maintains acoustic strength throughout the basin. The upper unit of section I is mostly transparent with numerous thinly spaced (decimeter scale), low-amplitude reflectors (Fig. 8). These reflectors decrease in amplitude from south to north. A single high-amplitude reflector is observed in the lower third of section I that appears to correlate with the

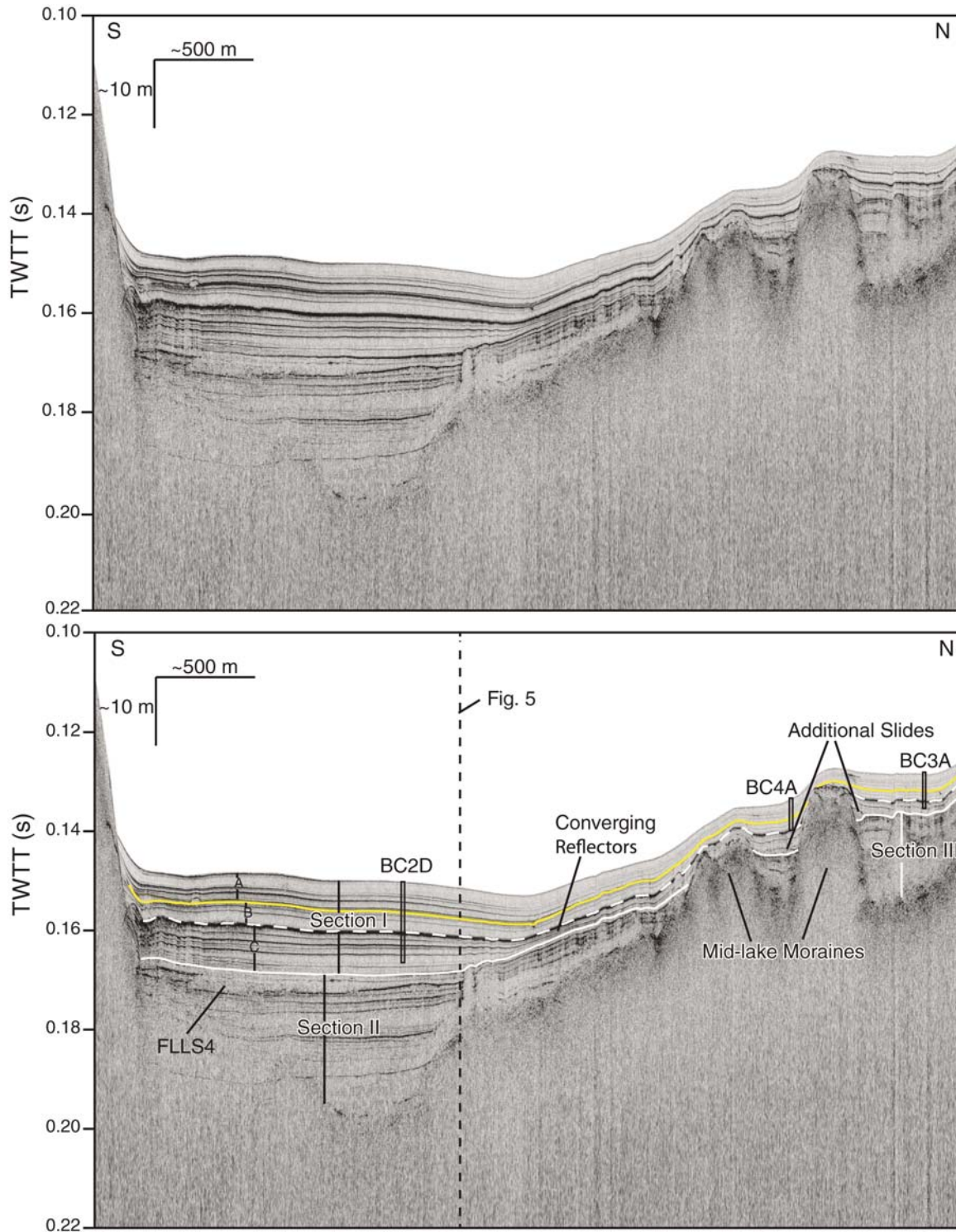


Figure 6. North-south-trending Chirp (compressed high intensity radar pulse) profile showing variability in character of sediment packages between the northern and southern parts of the basin, separated by the mid-lake moraines. The base of section I is marked in white, the Tsoyowata Ash horizon is dashed white, and the most recent event (MRE) horizon is marked in yellow. The Fallen Leaf Lake slide, FLLS1, is also in yellow where resolved. The location and penetration depth of piston cores BC2D, BC4A, and BC3A are illustrated. TWTT—two-way traveltime.

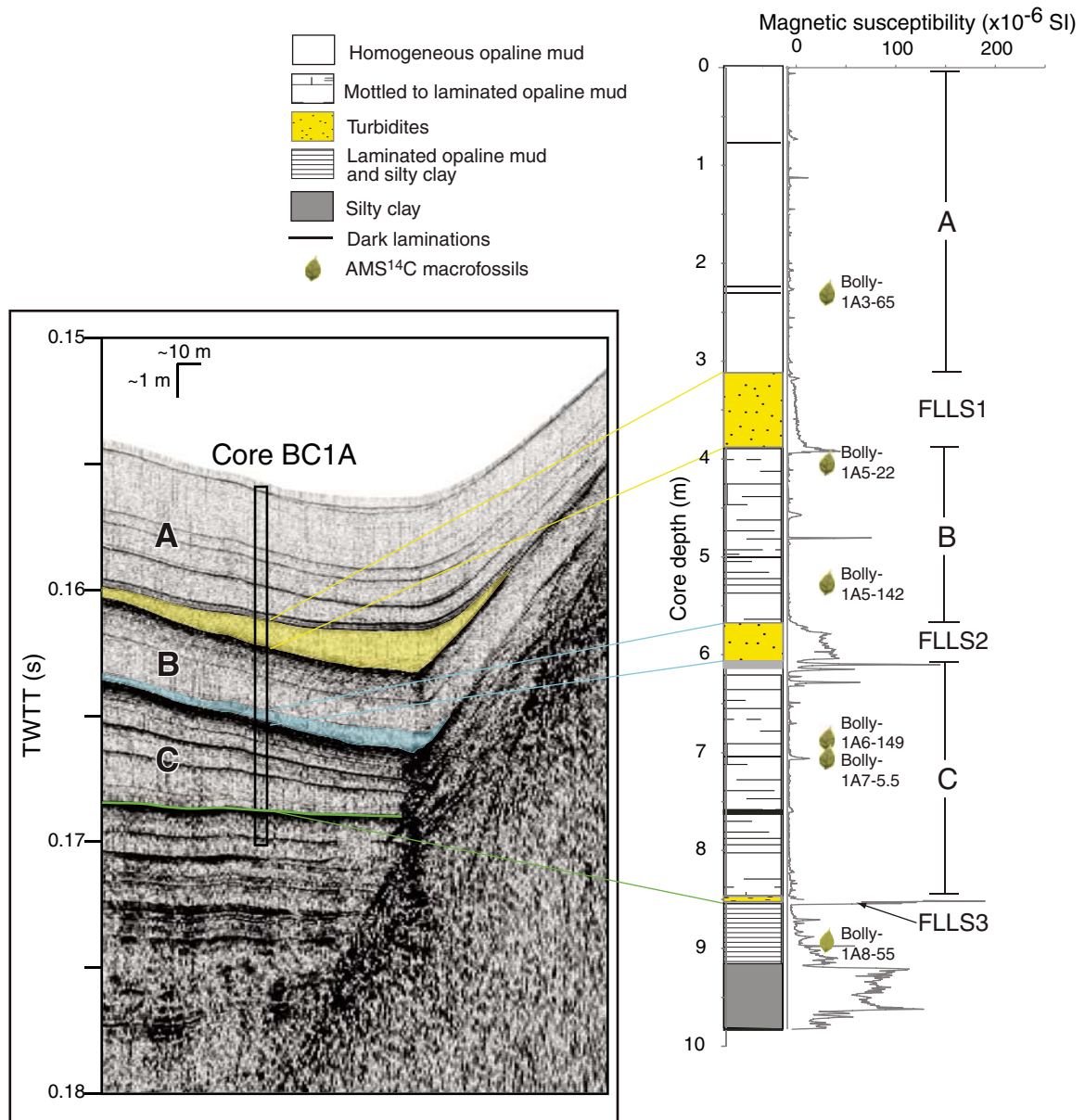


Figure 7. Enlargement of section from Figure 5 Chirp (compressed high intensity radar pulse) profile correlated to piston core BC1A. The three slide deposits observed in the core are easily identified in Chirp data and were used to correlate the core to the Chirp imagery. The three Fallen Leaf Lake slides are FLLS1 (yellow), FLLS2 (blue), and FLLS3 (green). See inset legend for detailed core lithology. Radiocarbon sample names are listed next to macrofossil symbols and correspond to dates from Table 1. TWTT—two-way traveltime; AMS—accelerator mass spectrometry.

base of a slide deposit. This reflector decreases in amplitude away from the slide deposit.

Along the base of the southern slope we observe two major strands of the WTDPF that trend ~N30°W (Fig. 8). The trend of the southern strand appears to extend onshore to the east and correlates with the trace of the WTDPF scarp identified in Lidar data (Fig. 2). Both strands produce offset of the lake floor, which increases downsection to the basement. It is difficult to

identify discrete offset of individual reflectors because of antecedent topography on the acoustic basement. However, the maximum observed offset on the northern strand is ~6.7 m at the lake floor and ~21.2 m at the acoustic basement. The maximum offset on the southern strand is ~7.5 m at the lake floor and ~17.8 m at the acoustic basement. Horizons are generally horizontal, but may exhibit some deformation as they approach the fault. The two strands become less well pro-

nounced to the northwest. In the northwestern most northeast-southwest-trending Chirp profile, we do not observe two distinct fault strands with obvious normal displacement, but rather several strands that deform basin sediments (Fig. 9). Some fault strands in this profile are characterized by chevron folds, while some exhibit normal displacement. This Chirp profile is located on the western slope of Cascade Lake and the steep topography may obscure significant offset

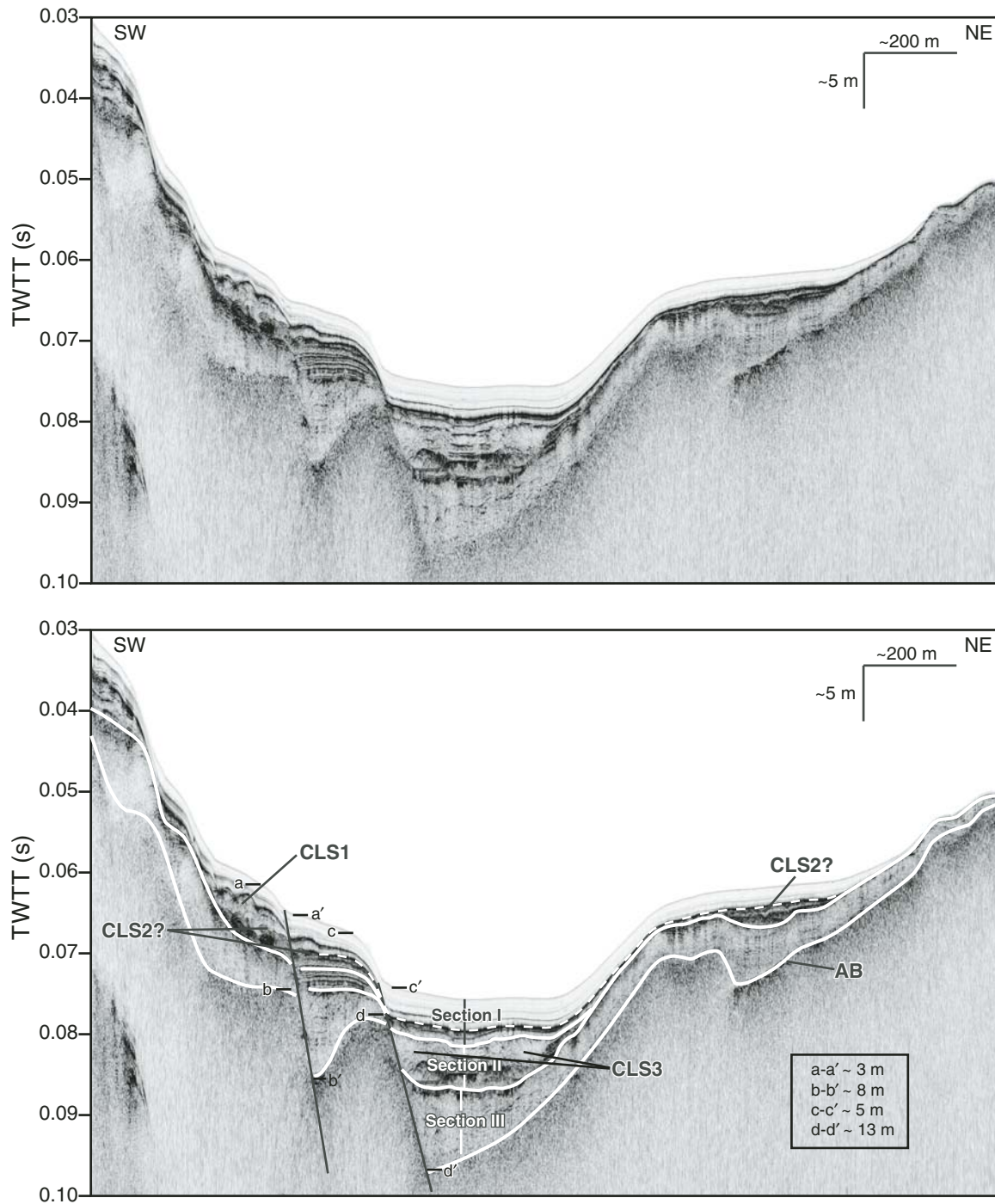


Figure 8. Southwest-northeast-trending Chirp (compressed high intensity radar pulse) profile from Cascade Lake (CL) illustrating two strands of the West Tahoe-Dollar Point fault (WTDPF) (solid black lines), slide deposits (CLS1, CLS2?, and CLS3), and acoustic character of lake stratigraphy. Offset on the two WTDPF strands is measured at the seafloor and the acoustic basement (AB) at locations indicated (a-a', b-b', c-c', and d-d'). The dashed horizon is interpreted to be synchronous with the Tsoyowata Ash horizon. Section boundaries are marked in solid white. TWTT—two-way traveltime.

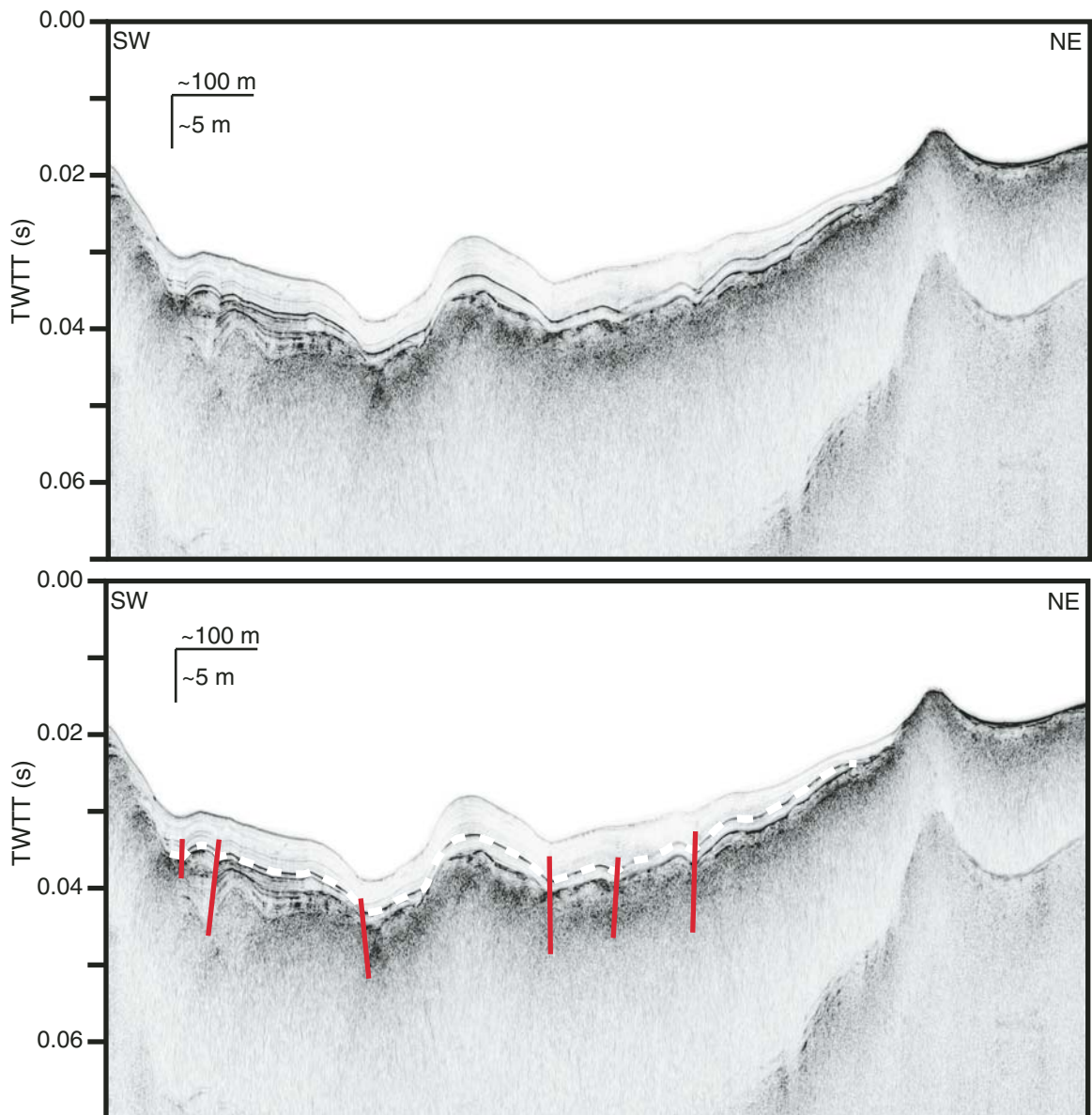


Figure 9. Westernmost Chirp (compressed high intensity radar pulse) profile in Cascade Lake. Strands of the West Tahoe–Dollar Point fault are shown in red. The faults are more distributed than in the central basin, with evidence of transtensional deformation. The dashed white line traces the interpreted Tsoyowata Ash horizon. TWTT—two-way travelttime.

of the acoustic basement observed in eastern profiles. The shallowest horizon deformed by these faults is a low-amplitude reflector within section I, which appears to correlate with a slide deposit (CLS1; CL is Cascade Lake). We did not identify strong evidence for a scarp extending onshore to the west from Cascade Lake in Lidar data (Fig. 2); the distributed nature of offset in Cascade Lake, along with no focused fault scarp observed west of the lake, may represent horsetail splaying of the WTDPF as it dies out to the west, toward Emerald Bay.

Emerald Bay

We use the same acoustic character observations in Fallen Leaf Lake and Cascade Lake to correlate the stratigraphy of Emerald Bay (Fig. 10). In general, section III is the oldest sediment that is characterized in large part by a chaotic acoustic character with some high-amplitude wavy and discontinuous reflectors. The acoustic character of section II is variably spaced low- to high-amplitude reflectors between semitransparent packages. Section I is mostly transparent with many low-amplitude

reflectors and a few higher amplitude reflectors. In Emerald Bay, the reflectors of section I generally decrease in amplitude from south to north; however, some locations show more lateral variation in acoustic amplitude.

Sediment core EB2 recovered from Emerald Bay penetrated to a depth of ~5.3 m below the lake floor, and 3 radiocarbon dates were determined (Table 1). We calculate a constant sedimentation rate of ~1 mm/yr between the youngest and oldest dated samples. The dates also suggest an increase in sedimentation rate

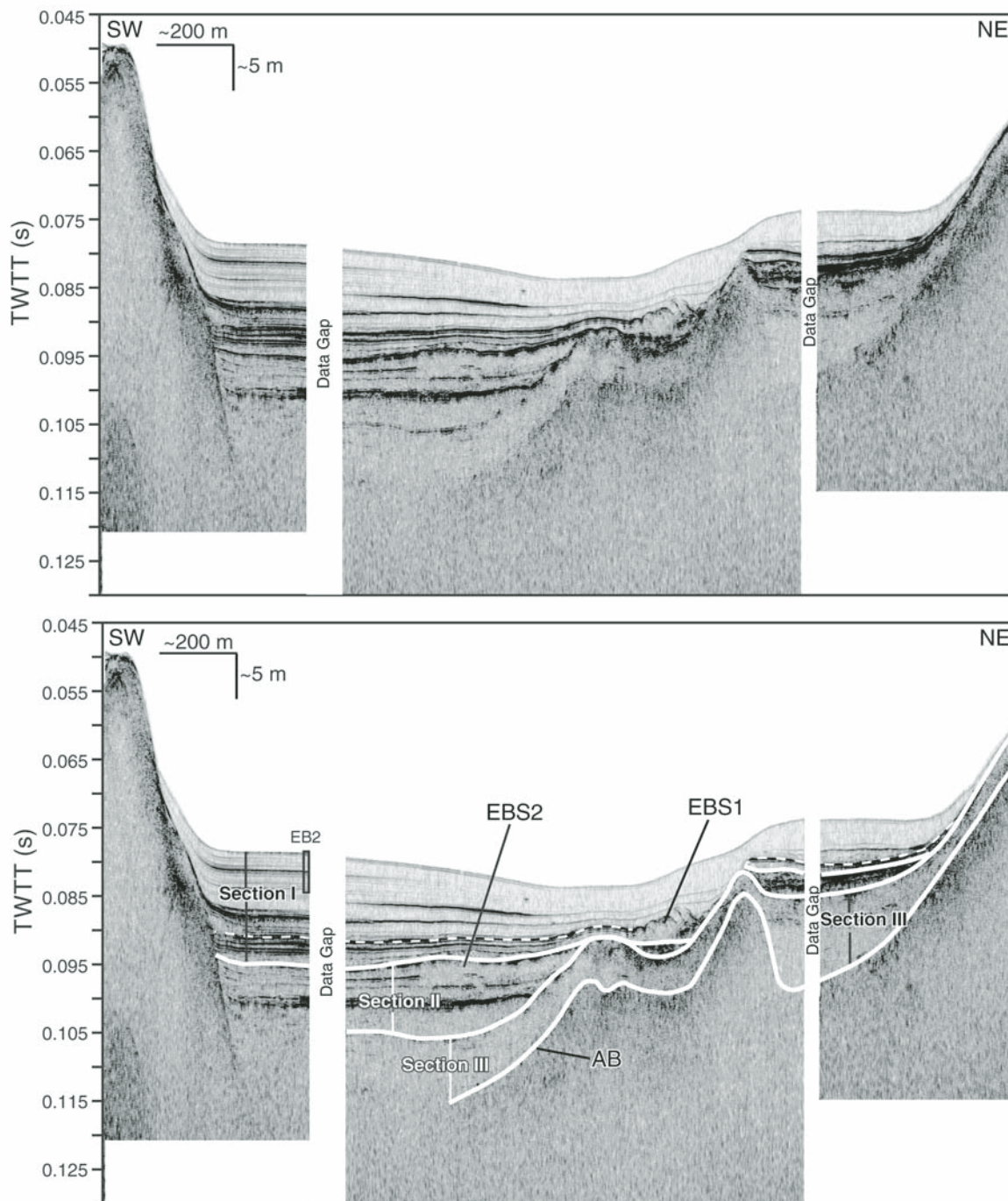


Figure 10. Southwest-northeast-trending Chirp (compressed high intensity radar pulse) profile from Emerald Bay (EB) showing acoustic character of the stratigraphy (sections I–III) and slide deposits (EBS1 and EBS2). The dashed line corresponds to horizon 1 in Figure 11, and is interpreted as the Tsoyowata Ash horizon based on acoustic correlation to Fallen Leaf Lake. Location and approximate penetration depth of piston core EB2 is also shown. Solid white lines mark section boundaries. In the southern basin, section II and III are not differentiated because a distinct boundary is not observed. The depth to acoustic basement (AB) is also not identified in the southern basin. TWTT—two-way travelttime.

with depth. Between the youngest samples, we calculate a sedimentation rate of ~ 0.99 mm/yr, but the time spanning the oldest samples yields a sedimentation rate as high as ~ 1.24 mm/yr.

The WTDPF is not readily observed in Chirp data from Emerald Bay (Figs. 10 and 11). Nevertheless, we observe acoustic wipeout to the northeast of the island located in the southern part of the bay (Fig. 11). In a single profile, we observe acoustic reflectors diverging to the

south, into the acoustic wipeout (Fig. 11). The diverging beds are not observed in the Chirp lines to the north or south. The youngest horizon that exhibits rotation and divergence into the gas wipeout is horizon 1. Although the sediment package between horizon 1 and horizon 2 thickens toward the gas wipeout, horizon 2 does not dip toward the south where it intersects the gas wipeout. Reflectors above horizon 2 are sub-horizontal and do not slope toward the south.

Event Deposits

Fallen Leaf Lake

We observe four recurring slide deposits in Chirp data and sediment cores from Fallen Leaf Lake: FLLS1, FLLS2, FLLS3, and FLLS4 (Fig. 12; Table 2). FLLS1 and FLLS2 are morphologically similar; both consist of a proximal and a distal component that have a measurable thickness in Chirp data (Fig. 13). FLLS3 and FLLS4 have proximal components that are discernible in Chirp data (Figs. 12C, 12D), but the distal component is too thin to be resolved. Nevertheless, FLLS3, manifested as a 4-cm-thick turbidite, was recovered in core BC3A and both slides may have distal components represented by high-amplitude reflectors. The proximal slides are identified in Chirp as chaotic, homogeneous units that disrupt previously deposited horizontal reflectors (Figs. 5 and 13). For all four slides, we are able to identify the youngest acoustic horizons disrupted by the proximal slides. These horizons also correlate to the base of the associated distal component for FLLS1 and FLLS2. In all cases, these slides correlate with strong reflectors that can be traced throughout the basin. The tops of the proximal slides are identified by a hummocky surface and a change from chaotic, homogeneous units below to transparent laminated units above (Fig. 13). The bases of the proximal slides are not always apparent due to acoustic attenuation and scattering.

FLLS1 was first identified and described by Brothers et al. (2009), who described the distal portion of the slide as a diverging unit that onlaps bathymetric highs, thickens into lows, and infills accommodation created during the MRE. The proximal slide, sampled by a piston core, is coarse grained and contains several large pieces of wood and smaller twigs. With the addition of new high-resolution Chirp data, we are able to map the extent of the proximal, massive slide deposits in more detail and calculate the thickness of the distal slide (Fig. 12). We observe two apparently synchronous proximal slide deposits located in the southwestern and southeastern corners of the lake. The maximum observed thickness of the proximal FLLS1 is ~ 3.9 m and the deposits cover a total area of ~ 0.40 km². The youngest acoustic horizon disrupted by FLLS1 is identified as the MRE horizon. The proximal slides appear to grade into the distal slide, which overlies the MRE horizon (Figs. 5 and 13). The distal slide is transparent in Chirp profiles and infills accommodation created by the MRE as well as other topographic lows (Fig. 5). The maximum thickness of the distal slide is ~ 1.9 m over the mapped extent (~ 2.08 km²; Fig. 12). The calculated areal extent is based on where the thickness of the deposit was detectable in

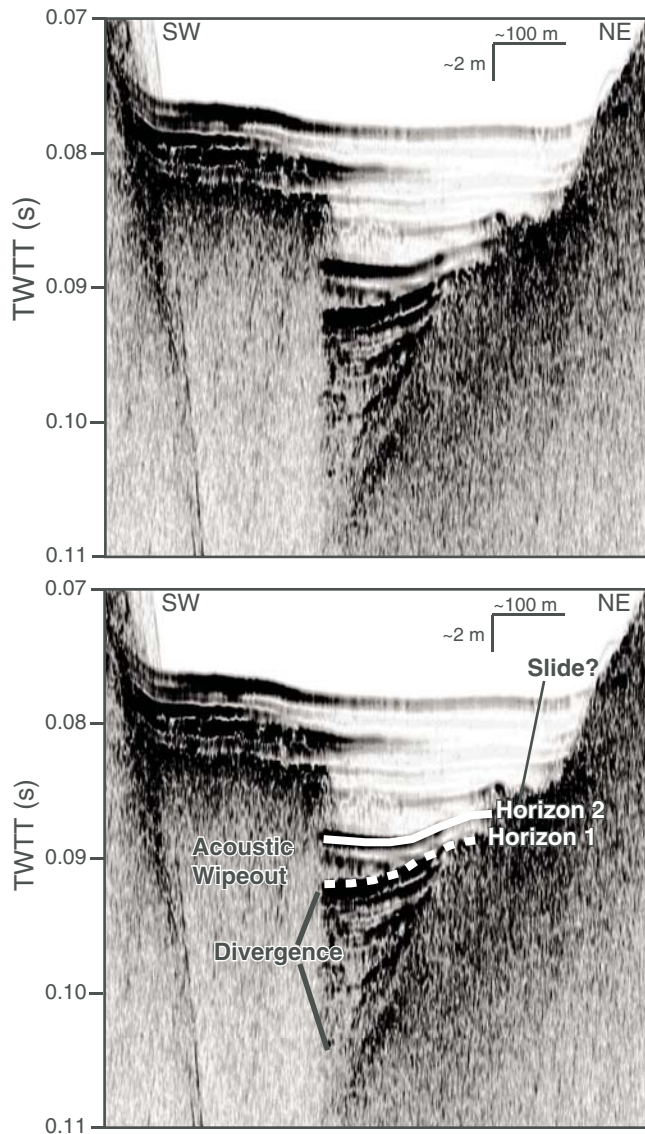


Figure 11. Southwest-northeast-trending Chirp (compressed high intensity radar pulse) profile beneath Emerald Bay images diverging beds. Horizon 1 is correlated to the dashed horizon in Figure 10, and is interpreted as the Tsoyowata Ash horizon. Above horizon 2, divergence is not observed. Acoustic basement at the far left of the profile slopes up toward the island in Emerald Bay. TWTT—two-way traveltime.

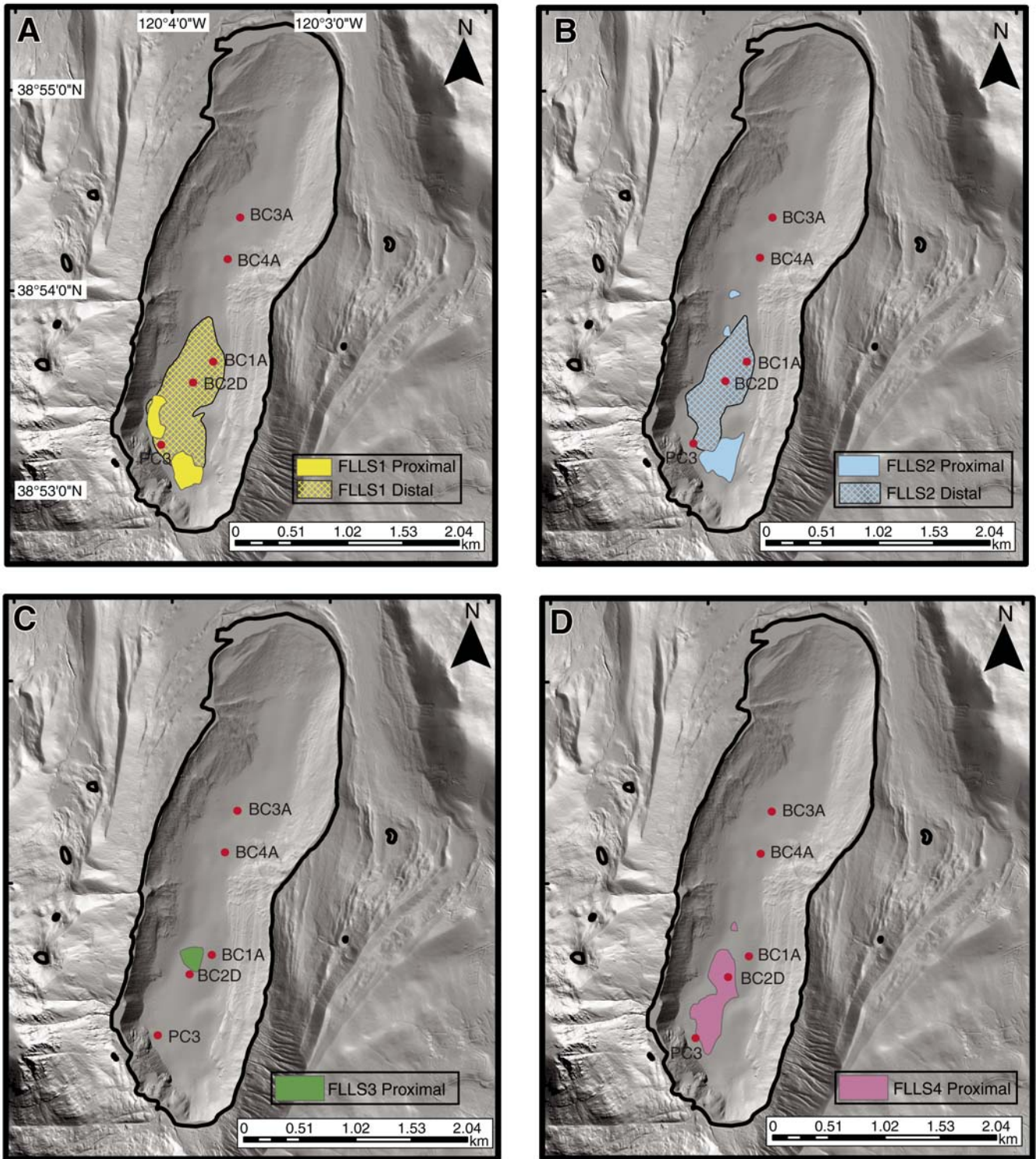


Figure 12. Locations of Fallen Leaf Lake slide deposits. (A) FLLS1. (B) FLLS2. (C) FLLS3. (D) FLLS4. Locations of piston cores are shown as red dots and labeled with core identifications.

Paleoseismic history of the Fallen Leaf segment of the West Tahoe–Dollar Point fault

TABLE 2. NAMES AND AGES FOR SLIDE DEPOSITS LISTED BY SUBBASIN

Approximate age (ka)	Lake Tahoe*	FLL	Emerald Bay	Cascade Lake
4.5	F	FLLS1	—	—
5.3	G	—	—	CLS1
8	J	FLLS2	EBS1	CLS2?
11.5	O	FLLS3	EBS2	CLS3
13	—	FLLS4	—	—

Note: FLL—Fallen Leaf Lake; dash indicates slide not observed.
*Data from Smith et al. (2013).

Chirp data and is therefore likely an underestimate. For example, the slide is sampled farther north in piston core BC3A, where it was recovered as an ~5-cm-thick deposit, below the Chirp detection limit. The horizon correlated to the base of the distal slide remains highly reflective throughout the basin, indicating that the slide may cover the entire area of the basin.

The FLLS1 distal slide mapped in Chirp data was correlated to piston cores, and radiocarbon dates were acquired for organic material bracketing FLLS1 in four different cores (cores BC3A, BC2D, BC1A, and PC3; Fig. 2; Table 1). The conservative age range of the slide determined from these dates is 2.89–5.69 ka, using the oldest and youngest modeled dates. The preferred age model, which is a composite model for all cores, constrains the age of FLLS1 to 4.57–4.85 ka (Fig. 14).

The FLLS2 slide directly overlies the Tsoyowata Ash marker bed. The Tsoyowata Ash was recovered in piston cores BC1A and BC2D and was correlated to Chirp data and mapped throughout the basin. The ash is 7.7–8.0 ka and was sourced from a Mount Mazama eruption (Bacon, 1983; Sarna-Wojcicki et al., 1991). In the piston cores, the distal portion of FLLS2 was recovered directly on top of the Tsoyowata Ash. In Chirp data, we observe both a massive, proximal slide and the associated distal deposits that were recovered in the cores (Figs. 5, 7, and 13). The proximal slide is located in the southwestern area of Fallen Leaf Lake, covering an area of ~0.35 km² (Fig. 12). The chaotic deposit disrupts horizontal reflectors that are folded adjacent to the margin of the deposit. The youngest disrupted horizon is correlated to the Tsoyowata Ash deposit. Although the base of the proximal slide is not always visible due to acoustic scattering and attenuation, the distal margin of the slide disrupts ~7.6 m of previously deposited sediment. In some areas, the slide unit contains fragments of folded and tilted horizons. None of the sediment cores penetrated the proximal section of FLLS2. We also image two local slides near the central basin that were deposited directly above the Tsoyowata Ash horizon (Fig. 12).

Similar to FLLS1, the distal portion of FLLS2 is acoustically transparent and infills topographic lows (Fig. 5). The maximum

thickness of the distal slide is ~1.0 m over the mapped extent (~1.37 km²). The FLLS2 distal slide appears to extend across the entire basin, was recovered as a <5 cm deposit in the northernmost core BC3A, and remains highly reflective throughout the basin.

Modeled radiocarbon ages for FLLS2 yield a conservative age range of 7.06–7.93 ka and a preferred age range of 7.62–7.90 ka (Table 1; Fig. 14). These results are based on dates from three piston cores bracketing the slide. The preferred model is a composite of dates from all three cores.

The proximal slide FLLS3 is imaged in Chirp data covering ~0.12 km² with a maximum thickness of ~1.3 m (Figs. 5 and 12). Slide FLLS3 appears to have a distal component that reaches at least 550 m across the lake, was recovered in core BC1A, is dated as ca. 11.24–11.64 ka, and is observed as a strong reflector in Chirp data.

Slide FLLS4 is observed in Chirp data as a massive, proximal slide deposit in the southern lake basin covering an area of ~0.72 km² (Figs. 6 and 12). A small slide is also observed along the western slope in the central basin, which may not be directly linked to the southern slide, but appears to have been synchronous (Fig. 12). In some areas, the top of the slide is not well defined by an acoustic reflector, but the base of the slide is often marked by a high-amplitude subhorizontal reflector. The character of the deposit is chaotic and the slide disturbs previously deposited horizontal reflectors. The maximum slide thickness is ~2.8 m. FLLS4 is chaotic, and returns from within the deposit are of lower amplitude than those observed in FLLS1 and FLLS2 proximal slides. FLLS4 is located near the center of the southern basin and along the western basin slope (Fig. 12). The youngest reflector disrupted by the slide can be traced throughout the basin; however, it is below the depth of the deepest penetrating piston core. To date this horizon, we extrapolated sedimentation rates observed in piston core BC1A, which yielded an age of ca. 13.2–16.3 ka (Table 1). The disrupted reflector used in the calculation is at the base of the slide and therefore the slide may be slightly younger than calculated.

We also observed several small, isolated slide deposits in northern Chirp profiles (Fig.

6). These slides do not appear to have a distal component. Stratigraphy is highly condensed in northern lake sediments, making it difficult to trace horizons continuously to the north. The slides are stratigraphically below the FLLS1 and FLLS2 horizons and may correlate with the older slides observed in the southern basin. The slide deposits occur near a distinct transition in the seismic stratigraphy of the northern basin between homogeneous, chaotic units below (section III) and thinly bedded, acoustically transparent layers above (section I). As such the northern slides may be correlated to one another. The combined area covered by these deposits is ~0.15 km².

Cascade Lake

We observe two major slide deposits in Cascade Lake (Fig. 8). The youngest slide, CLS1, is located at the base of the steep southern basin slope. The slide is between the two strands of the WTDPF and across the southern strand to the south. Slide CLS1 has a hummocky upper surface below the transparent sediments of section I. The slide covers an area of ~0.1 km² and reaches a maximum thickness of ~2.1 m. CLS1 marks the uppermost high-amplitude reflector of section I. Even though the WTDPF makes direct tracing of this horizon difficult, we assume, on the basis of acoustic character, that the horizon north of the WTDPF corresponding to the slide is also the uppermost high-amplitude reflector. This allows us to compare the age of the slide with slide CLS3. Slide CLS3 comprises two apparently synchronous slides (Fig. 8); both have similar acoustic characteristics and so are described as one. CLS3 is stratigraphically lower than CLS1, and is located north of both strands of the WTDPF in the depocenter of the lake. The slide is acoustically chaotic with a hummocky surface. It disturbs several horizons within section II sediments. The uppermost horizon disturbed by CLS3 was used to determine the relative age of the slide. CLS3 covers ~0.09 km² and has a maximum thickness of ~3.8 m.

Emerald Bay

We observe two major slide deposits in sediments beneath Emerald Bay (Fig. 10). The youngest slide, EBS1, has a hummocky upper contact with transparent to laminated units above and a maximum thickness of ~4.5 m. The slide is acoustically chaotic, disturbs previously deposited horizons, and covers an area of ~0.06 km². The uppermost horizon disturbed by EBS1 is a reflector that maintains a high-amplitude signal throughout the basin, and corresponds to horizon 1 in Figure 11. The slide is located in the central basin near the base of the gently northeast sloping acoustic basement

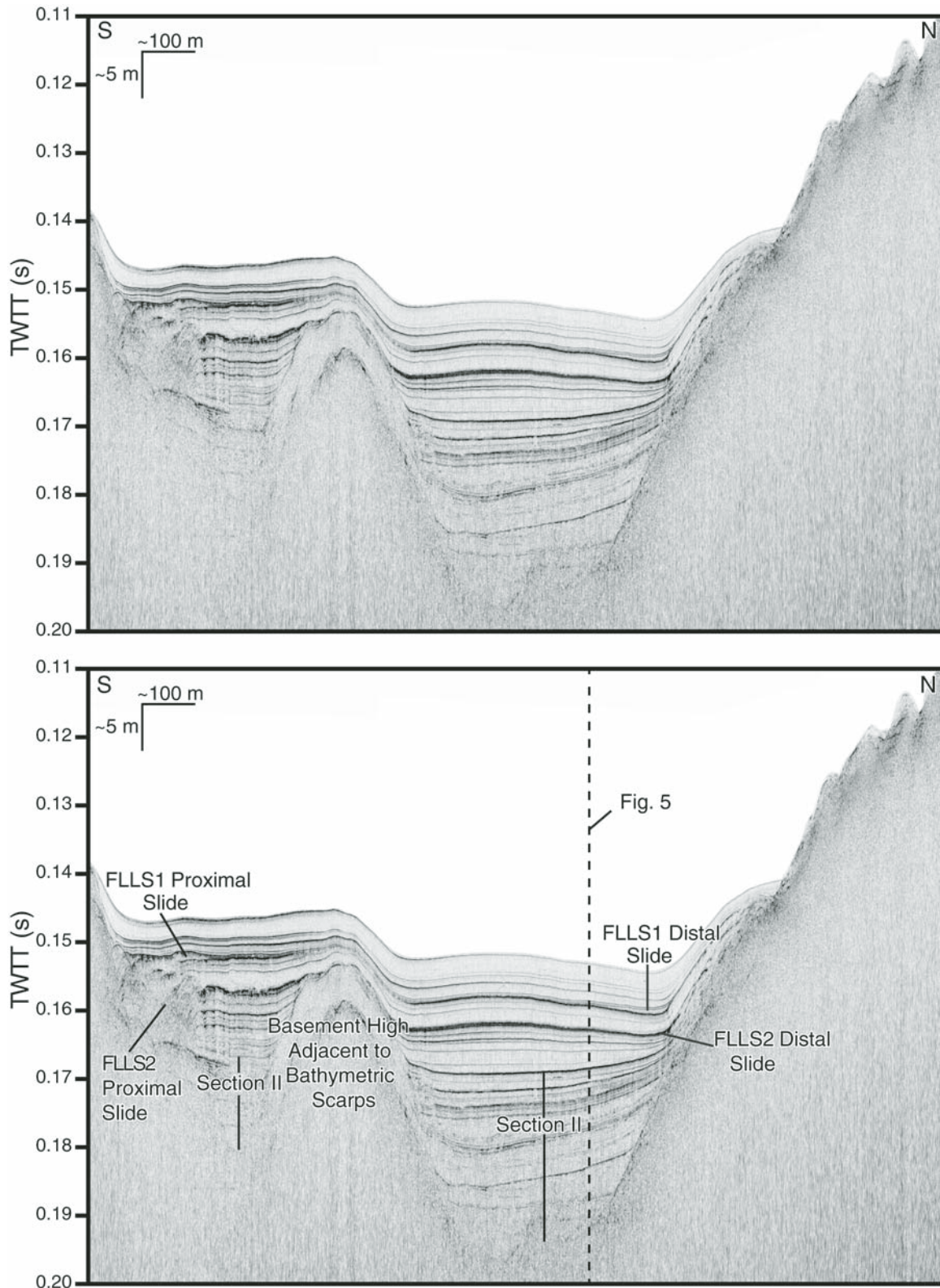


Figure 13. North-south-trending Chirp (compressed high intensity radar pulse) profile from Fallen Leaf Lake showing proximal and distal FLLS1 and FLLS2 slides. TWTT—two-way traveltime.

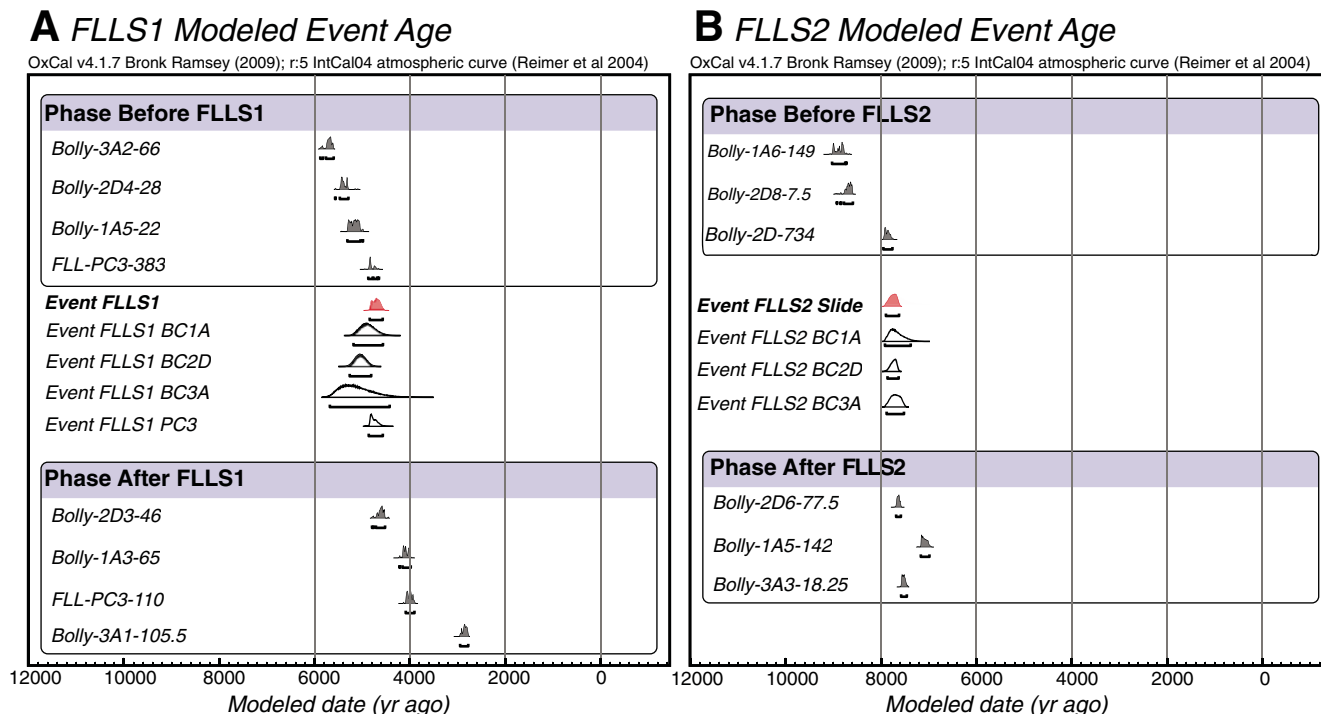


Figure 14. (A) The modeled event age of Fallen Leaf Lake slide FLLS1. (B) The modeled event age of FLLS2. The probability distribution for each radiocarbon date is shown in gray, the modeled dates for individual cores are white, outlined in black, and the combined preferred model is shown in red. Additional information on radiocarbon dates is available in Table 1.

horizon. The older slide, EBS2, is similar in character to EBS1 and is located slightly to the southeast (Fig. 10). The maximum thickness of slide EBS2 is ~2.9 m and it covers an area of ~0.26 km².

By extrapolating below the bottom of sediment core EB2 using a 1 mm/yr sedimentation rate and accounting for potential uncertainty due to overpenetration of as much as 0.5 m, we constrain EBS1 as ca. 9.4–10.2 ka, and slide EBS2 as ca. 12.7–13.5 ka. Using the radiocarbon ages from core EB2, we calculate a sedimentation rate of ~0.99 mm/yr between the two youngest dates and an increase in sedimentation rate to ~1.24 mm/yr between the two oldest dates. This increase in sedimentation rates observed down-core should continue, as glacially derived sediment sources would have been closer. In addition, during the Tioga glacial period, glaciers would have eroded previously deposited sediments and ice would have been in contact with the Chirp acoustic basement horizon. A thickness of >25 m of sediment is observed above the acoustic basement at the location of EB2. If the acoustic basement represents the retreat of the last Tioga glacial period (ca. 14 ka), this would require a faster sedimentation rate to account for >25 m of sediment accumulated at this location. Furthermore, we observe an increase in sedi-

mentation rate with depth in Fallen Leaf Lake sediments, and we expect these two basins to have somewhat similar patterns in sedimentation. If we use the increased sedimentation rate of ~1.24 mm/yr below the bottom of core EB2, we obtain age ranges for EBS1 of ca. 8.6–9.3 ka and for EBS2 of ca. 11.2–11.9 ka.

DISCUSSION

Stratigraphic Interpretation

The Tioga glaciation, which lasted from ca. 30 to ca. 14 ka, consisted of several cycles of glacial advance and retreat (Benson et al., 1998; Bischoff and Cummins, 2001; Clark and Gillespie, 1997; Phillips et al., 1996; Rood et al., 2011). The series of arched terminal and recessional Tioga moraines that bound Fallen Leaf Lake, Cascade Lake, and Emerald Bay to the north (Saucedo et al., 2005) delineate the farthest advance of Tioga glaciation. The mid-lake moraine complex, mapped in Fallen Leaf Lake Chirp data, was likely deposited during a stillstand in glacial retreat or a subsequent, less extensive advance. The ridges observed in the Chirp acoustic basement horizon align with ridges observed in lake bathymetry and with mapped Tioga-age moraines onshore. These

moraines created topography on the basin floor that has affected sedimentation patterns in Fallen Leaf Lake.

We assume that the glaciers that formed Fallen Leaf Lake, Emerald Bay, and Cascade Lake were in contact with the acoustic basement during the Tioga glaciation. Therefore, the sedimentary packages above the acoustic basement were deposited after the retreat of the glaciers from these lakes at the end of the Tioga glaciation, ca. 14 ka. In Fallen Leaf Lake, the basin also records stalls in the glacial retreat as evidenced by the mid-lake moraines. Section III infills lows created by the mid-lake moraine complex (Fig. 6); we interpret these deposits as subglacial or proglacial deposits. The chaotic and strongly reflective acoustic nature of these deposits is consistent with such a depositional scenario and suggests that they are coarse grained and lack internal structure. Some horizons can be distinguished and may represent coarser material deposited as an outburst flood event (e.g., Uchupi and Ross, 2000). Section III is only observed north of the mid-lake moraines, but similar deposits may be deeper than the penetration capability of Chirp data in the southern basin. We interpret section III as the oldest sedimentary section deposited when the glacier extended to the mid-lake moraines.

Subsequent to deposition of section III, the glacier retreated up the valley, and sedimentation of section II began in the deep accommodation created by the glacier and the WTDPF in the southern basin. We interpret section II as sediment carried by glacial meltwater and deposited in a proglacial lake (Figs. 5, 6, and 7). Sedimentation rates were high during deposition of section II as the rapidly melting glacier carried sediment to the basin. The age of the upper contact of section II is ca. 11.24–11.64 ka and the maximum thickness of section II is >40 m, indicating an average sedimentation rate of ~16 mm/yr. Furthermore, the onlap of layers within section II onto basin slopes is flat and subhorizontal, and horizons maintain a strong acoustic amplitude laterally throughout the section. This may indicate rapid emplacement of gravity flows from glacial outburst floods. Section II sediments are not observed north of the mid-lake moraine complex; however, it is possible that we are not able to separate a highly condensed section II from section I or III. These topographic highs may have acted as depositional barriers for sediments that mainly entered the basin from the south.

The upper contact of section II appears to mark the transition from glacial deposits below to lacustrine sediments in section I above. This transition was captured in core BC1A, where we observe glacial silt and high magnetic susceptibility below the upper contact of section II, and lacustrine sediments and low magnetic susceptibility above the upper contact of section II (Fig. 7). In Chirp data, a change from uniform thickness and flat onlap at basement highs to lenticular deposits that onlap high onto basement walls also suggests a change from glacial to lacustrine deposition (Fig. 5). The diminished acoustic amplitude of reflectors to the north indicates that the source of sediment for section I was primarily from the south.

In Cascade Lake and Emerald Bay, we do not observe the lenticular pattern of section I, but are able to correlate the sections based on acoustic character. Section I in Emerald Bay and Cascade Lake is primarily identified by characteristic onlap high at basin walls. Section I in these basins has high-amplitude reflections near the base, but is mostly transparent in the upper sediments. As with section I in Fallen Leaf Lake, we interpret these deposits to be lacustrine deposits. Section II and section III are considered glacial deposits, similar to those of Fallen Leaf Lake. Section III is the older of the units, and the entire sequence from section III through section II is interpreted to be a transition from subglacial, to proximal proglacial, to distal proglacial deposits.

Character of Slide Deposits

The slide deposits observed in Fallen Leaf Lake sediments are characteristic of debris flow and turbidite deposits. The FLLS1 and FLLS2 slides are indicative of large proximal debris flow deposits with associated distal turbidites. The turbidite deposits are easily identifiable in Fallen Leaf Lake cores as graded beds, and they infill lows in topography created by scour and differential deposition observed in section I. We observe only a proximal debris flow component for FLLS3 and FLLS4 in Chirp data, though both slides correspond to a high-amplitude reflector that maintains strength throughout the basin and may represent the distal components.

The FLLS1 proximal slides appear to be sourced from the southeastern and southwestern corners of Fallen Leaf Lake (Fig. 12). Although we do not observe evidence for well-defined deltas, these are both areas of water and sediment input to the lake. The southeastern slide is located near the Glen Alpine Creek input and the southwestern slide is located near several small, unnamed creeks that drain from the steep slopes of Cathedral Peak (Fig. 2). The southwestern slide may be sourced from the small apron extending slightly onto the basin floor from the slope. Above the slope is a set of ridges that may be scarps from the FLLS1 slide (Fig. 3). The large FLLS2 proximal slide also appears to be sourced from the southeastern area of the lake near the Glen Alpine Creek input (Fig. 12). The southern source area for the FLLS1 and FLLS2 slides is also adjacent to the WTDPF and the steepest basin wall slopes, where slide deposits triggered by an event on the fault would be expected. The two smaller proximal slides associated with the FLLS2 deposits are located near the Cathedral Creek input to the lake on the western shore (Fig. 12). FLLS3 is sourced from the western slope, just south of the input from Cathedral Creek (Fig. 12). FLLS4 extends throughout much of the southern basin. In the south, the source of the slide appears to be the southern slope, whereas to the north the source appears to be the western slope, near Cathedral Creek (Fig. 12). This suggests that the FLLS4 may be two distinct slides that coalesce near the center of the southern basin. Several slides were sourced from the western slope near Cathedral Creek. This is directly below two slide deposits mapped onshore that are adjacent to the WTDPF trace (Saucedo et al., 2005). In Lidar data, the toe of the eastern slide is located on the footwall side of the fault trace (Fig. 2). The westernmost slide is larger and is deposited across the trace. We do not observe a fault trace across the western slide deposit, so either the slide occurred

post-MRE, or is difficult to observe across the hummocky, coarse slide deposit. It is also possible that the slide was synchronous with the MRE, but we lack sufficient data to determine an age. We also cannot determine if these slides were synchronous with older slide deposits in Fallen Leaf Lake.

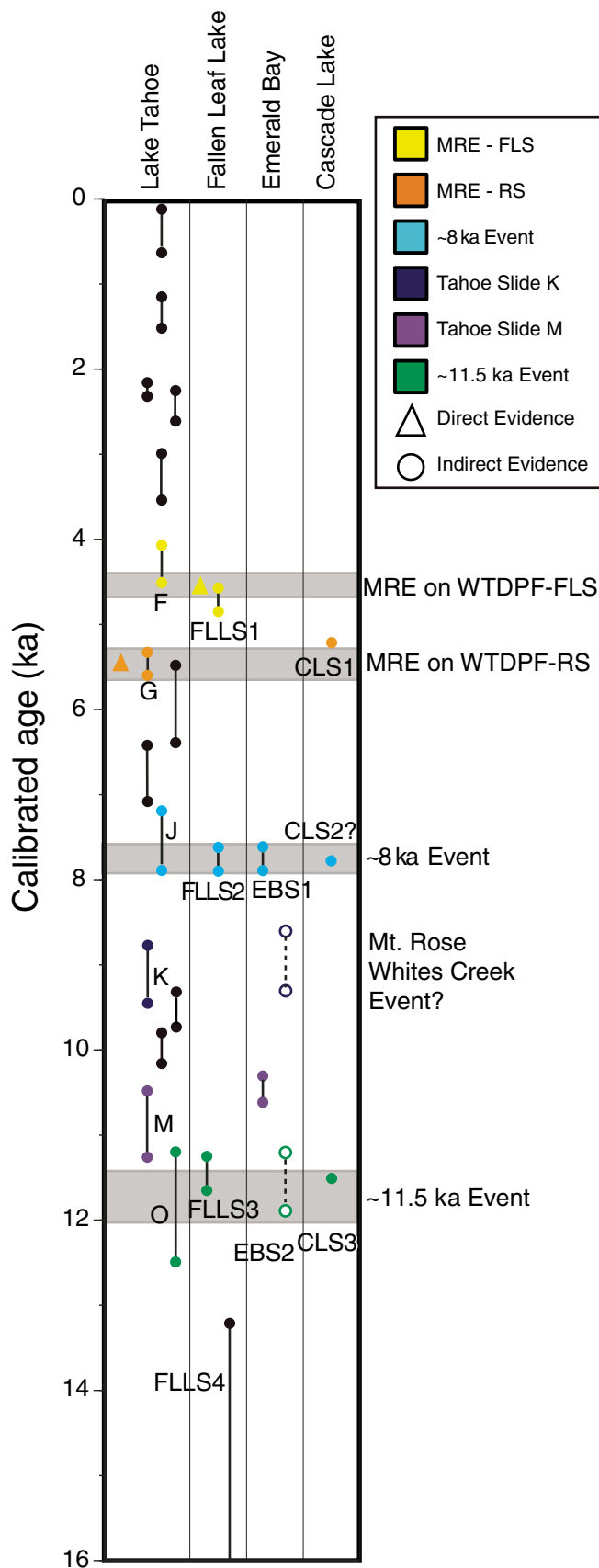
In Emerald Bay, the slide deposits appear sourced from the northwestward-sloping basin wall; this is toward the mouth of the bay. A slide is mapped onshore spilling into the southern part of Emerald Bay (Saucedo et al., 2005), but we do not observe a slide sourced from this area in Chirp data. In Cascade Lake, CLS1 appears to be sourced from the southern slope on the footwall of the WTDPF. CLS3 is deposited in the basin depocenter and appears to be sourced from both the northern and southern basin slopes. An onshore slide is also mapped at the southernmost shore of Cascade Lake (Saucedo et al., 2005). In Lidar data the onshore slide is directly adjacent to the WTDPF on the footwall side of the trace (Fig. 2). With currently available data, it is difficult to determine if the onshore slide is related to any of the slides observed in Chirp data.

Timing of Slide Deposits

Age ranges for the slide deposits observed in Lake Tahoe (Smith et al., 2013), Fallen Leaf Lake, Emerald Bay, and Cascade Lake are plotted in Figure 15. The ages of dated slide deposits in Emerald Bay and Cascade Lake are estimates and more detailed radiocarbon dating is needed to confirm temporal correlations with slides in Fallen Leaf Lake and Lake Tahoe. Although the ages of the Emerald Bay and Cascade Lake slides are estimated from acoustic correlation, we have more confidence in slide deposit dates for Fallen Leaf Lake, which are based on a robust age model (Table 1; Fig. 14).

The age model determined from the 2010 piston cores in Fallen Leaf Lake constrains the age range of FLLS1 as 4.57–4.85 ka. We suggest that FLLS1 in Fallen Leaf Lake is synchronous with the MRE on the WTDPF Fallen Leaf Lake segment and event deposit F in Lake Tahoe (4.07–4.51 ka; Smith et al., 2013). Deposit F is characterized by a debris flow and multiple turbidites that appear to originate from, and are constrained to, the northern Lake Tahoe Basin (Smith et al., 2013). Despite the slight difference in estimated age ranges, we suggest that deposit F and FLLS1 were both triggered by the same seismic event on the Fallen Leaf Lake segment of the WTDPF. Given the preferred age models for deposit F and FLLS1, the age of this event is ca. 4.5 ka. Errors in the modeled age range of FLLS1 or deposit F in Lake Tahoe could be due

Paleoseismic history of the Fallen Leaf segment of the West Tahoe–Dollar Point fault



to sparseness of dates in pre-2010 cores, uncertainty in model calculations, or nonuniform deposition rates at the sites. Based on core data and seismic stratigraphy, there is no evidence for a young slide in either Emerald Bay or Cascade Lake that correlates with FLLS1.

The age model for FLLS2 in Fallen Leaf Lake constrains the age of the slide to 7.62–7.90 ka. In sediment cores, the distal component of FLLS2 is observed directly above the Tsoyowata Ash deposit; the ash bed provides a distinct marker bed to correlate with other subbasins. In Lake Tahoe, the age range for the synchronous deposit J is 7.19–7.89 ka (Smith et al., 2013). Deposit J also overlies the Tsoyowata Ash in cores from Lake Tahoe and is characterized by multiple debris flows originating along the southwestern basin and a single turbidite deposit that extends to the central and northern basin. Both FLLS2 and deposit J are characterized by large proximal slides relative to basin

←
Figure 15. Plot showing timing of direct (fault offset) and indirect (slide deposits) evidence for earthquakes in Lake Tahoe, Fallen Leaf Lake (FLL), Emerald Bay (EB), and Cascade Lake (CL). Where evidence is correlated across basins, the symbols are color coded by event age (see legend; MRE—most recent event; FLS—Fallen Leaf segment; RS—Rubicon segment). Black symbols represent evidence not correlated across multiple basins. The approximate ages for observed direct earthquake deformation on the Fallen Leaf Lake and Rubicon segments of the West Tahoe–Dollar Point fault are shaded in gray and marked with triangles. Proposed events based on synchronous slides across basins are also shaded in gray. All Lake Tahoe slides are modeled event dates (name convention is from Smith et al., 2013). The two youngest Fallen Leaf Lake slides are modeled event dates. The age range of the two oldest slides was calculated by extrapolating the age model for core BC1A. Two models of Emerald Bay event age ranges are shown. The solid symbols represent ages based on stratigraphic interpretation where EBS1 is synchronous with the FLLS2 and assigned the same age range of 7.62–7.90 ka. The EBS2 age is calculated based on a sedimentation rate of 1.24 mm/yr below EBS1. The dashed symbols were determined based on calculated sedimentation rates from core EB2 (see text). Cascade Lake event ages were determined based on acoustic character correlation with Emerald Bay and Fallen Leaf Lake.

size and turbidite deposits that extend laterally in each basin.

Based on a comparison of the stratigraphy between Fallen Leaf Lake, Lake Tahoe, Emerald Bay, and Cascade Lake, it is possible that slides observed in Emerald Bay or Cascade Lake are synchronous with FLLS2 and deposit J. The stratigraphic horizon representing slide EBS1 appears to mark a transition in acoustic character. Below the slide, we observe alternating semitransparent layers and high-amplitude reflectors. Above the slide we observe a more transparent unit with low-amplitude reflectors and a few high-amplitude reflectors (Fig. 10). In Lake Tahoe, Chirp data interpreted by Smith *et al.* (2013) illustrates that deposit J (7.19–7.89 ka) marks this same acoustic transition. In Fallen Leaf Lake, the transition to acoustically transparent units is less clear; we observe several high-amplitude reflectors even in the youngest units. In the northern part of the basin, where the sedimentary section is more condensed, the transition to transparent units is more apparent. In the northern basin, unit C of section I has several closely spaced, medium- to high-amplitude reflectors, while units A and B above have fewer, and lower amplitude, reflectors. This difference between unit C and units A and B is also observed where the basement slopes up to the north near the mid-lake moraine complex (Fig. 6). In this area, unit C more closely resembles section II below than units A and B above. The upper contact of unit C is the FLLS2 distal deposit. Based on the similar transitions in acoustic character in Emerald Bay, Fallen Leaf Lake, and Lake Tahoe, slide EBS1 appears to be correlated with FLLS2 in Fallen Leaf Lake and deposit J in Lake Tahoe. This is a reasonable assumption given the estimated age of ca. 8.6–9.3 ka calculated from core EB2. A slightly greater increase in sedimentation rate than predicted would shift the age of the slide toward the younger age of FLLS2.

Following this stratigraphic interpretation in Cascade Lake, we interpret the youngest, strong reflector that can be traced basin wide as the Tsoyowata Ash horizon (dashed horizon in Fig. 8). This reflector is actually resolved as two closely spaced high-amplitude reflectors in some parts of the basin. This is consistent with the Tsoyowata Ash horizon in Fallen Leaf Lake Chirp data. In Fallen Leaf Lake, two closely spaced high-amplitude reflectors may define the ash layer, with a lower amplitude reflector above marking the top of the FLLS2 turbidite. Several closely spaced, high-amplitude reflectors characterize the unit below this Tsoyowata Ash horizon in Cascade Lake, similar to the Emerald Bay stratigraphy. Using this correlation, slide CLS1 is younger than the FLLS2, and CLS3

is older than FLLS2. Nevertheless, we cannot rule out the presence of a slide associated with the Tsoyowata Ash horizon. There is some evidence that the youngest slide may obscure an older slide (CLS2?) below (Fig. 8). This interpretation of the Tsoyowata Ash horizon results in a sedimentation rate of ~ 0.39 mm/yr for sediments above the horizon in the deep southern basin. This would generate an age estimate for the younger slide of ca. 5.2 ka. This age is close to the age range of deposit G in Lake Tahoe (5.3–5.6 ka), which was associated with the age of a drowned tree near Baldwin Beach in Lake Tahoe and the MRE on the Rubicon segment of the WTDPF (Smith *et al.*, 2013).

The FLLS3 and FLLS4 slide age ranges are ca. 11.24–11.64 ka and ca. 13.2–16.3 ka, respectively. FLLS3 is synchronous with deposit O in Lake Tahoe, which was dated as 11.1–12.49 ka (Smith *et al.*, 2013). In addition, both event deposits mark the transition between bluish glacial silt and organic laminae below to olive lacustrine silt and clay above. The turbidite component of deposit O was mapped throughout Lake Tahoe above a major liquefaction feature, and the associated debris flow was mapped in the south-central part of the basin (Smith *et al.*, 2013). The older FLLS4 deposit is observed within Fallen Leaf Lake glacial sediments of section II. Although slide deposits older than deposit O were identified in Lake Tahoe, dates were not determined for these slides and it is therefore difficult to correlate FLLS4 to a slide in Lake Tahoe.

We can also estimate the ages of the older slides in Emerald Bay and Cascade Lake based on calculated sedimentation rates and stratigraphic correlations. In Emerald Bay, the previously estimated age of EBS2 is ca. 11.2–11.9 ka, which correlates with FLLS3 and deposit O in Lake Tahoe. The stratigraphy also suggests that this horizon may mark a transition from glacial sediments below to lacustrine sediments above, providing further evidence that the slide is synchronous with FLLS3 and deposit O. If the younger slide is ca. 8 ka and the older slide is ca. 11.5 ka in Emerald Bay, this yields a sedimentation rate between the two slides of ~ 0.95 mm/yr. This rate is slightly lower than rates determined for younger sediments in Emerald Bay, and is not consistent with the increase in sedimentation rate calculated downcore in EB2. This suggests that either our assumption of increasing sedimentation rates is incorrect, or our stratigraphic correlation is incorrect. An alternative interpretation would be that the transition to glacial sediments is deeper than EBS2, which would make EBS2 younger than FLLS3 and deposit O (solid circles and lines in Fig. 15). It is also plausible that EBS2 represents the

transition from glacial sediments; this would indicate that the age of EBS1 is slightly older than FLLS2 and deposit J (hollow circles and dashed lines in Fig. 15). Longer piston cores and more detailed radiocarbon dating are necessary to constrain further the ages of Emerald Bay slide deposits.

CLS3 appears to be synchronous with a transition in seismic stratigraphy. Deposits above the slide horizon appear to drape high onto basin walls, whereas sediments below the horizon are observed only in topographic lows with slight onlap onto basin highs. We interpreted this change to represent the transition from glacially derived sediment input to more pelagic lacustrine sedimentation. A similar shift is observed in Fallen Leaf Lake stratigraphy associated with the top of section II and FLLS3. Assuming that our pick for the Tsoyowata Ash horizon in Cascade Lake is correct and CLS3 is synchronous with FLLS3, we calculate a sedimentation rate between the Tsoyowata Ash horizon and CLS3 of 0.44–0.48 mm/yr. This range is reasonable given the sedimentation rate of ~ 0.39 mm/yr previously calculated for sediments younger than the Tsoyowata Ash horizon.

Triggering of Slide Deposits

There are several possible triggering mechanisms for the Tahoe Basin slide deposits, including lake-level fluctuations, storms, and earthquakes. There is evidence that Fallen Leaf Lake has undergone significant droughts and major changes in lake level during the mid- to late Holocene; these droughts may have occurred every 650–1150 yr (Kleppe *et al.*, 2011). Submerged paleoshorelines and upright and rooted trees observed below the lake surface suggest that lake level may have dropped 40–60 m below present elevation during the late Holocene (Kleppe *et al.*, 2011). The region has also undergone longer term climatic variability throughout the Holocene (Benson *et al.*, 2002), which may have affected Fallen Leaf Lake sedimentation patterns and induced lake-level fluctuations. Significant drops in lake level may trigger landslides by exposing upper slope deposits to wave action and shifting the location of water and sediment input. Although lake level has fluctuated greatly in Fallen Leaf Lake, we do not think that FLLS1 and FLLS2 were triggered by this mechanism. The submerged trees in Fallen Leaf Lake are dated as ca. A.D. 1250 (Kleppe *et al.*, 2011), but we do not observe major slide events of this age in Fallen Leaf Lake. In addition, lake-level fluctuations likely have occurred with a much shorter recurrence interval than the recurrence interval observed for slides in Fallen Leaf Lake; this evidence, together with coincident

Paleoseismic history of the Fallen Leaf segment of the West Tahoe–Dollar Point fault

slides in Lake Tahoe, suggests a regional trigger for the slides observed in the lake.

Storms are another possible triggering mechanism for slides in Fallen Leaf Lake. Storms may be associated with flooding and increased sediment input to the lake as well as wave erosion and loading in shallow water. Flooding associated with storms may cause hyperpynical flows, rapid accumulation, oversteepening, and pore pressure loading near stream mouths, all of which may lead to failures. Furthermore, waves associated with storms may erode nearshore sediment and generate hyperpynical flows, or may increase pore pressure and weaken slopes due to loading. As with lake-level fluctuations, we anticipate the recurrence interval of major storms to be much shorter than the interval determined for Fallen Leaf Lake slide deposits.

Seismic triggering is also a possible cause of the slides observed beneath Fallen Leaf Lake. Earthquakes may trigger slides by strong shaking, increased pore pressure due to ground motion, gas escape, and dropdown of the hanging wall that influences slope stability and lake level. The Fallen Leaf Lake segment of the WTDPF is directly identified beneath Fallen Leaf Lake and Cascade Lake and presumably extends (and dies) into southern Emerald Bay, as evidenced by localized diverging beds. The source area for FLLS1, FLLS2, and FLLS4 appears to be the steep WTDPF scarp that forms the southern basin wall. The correlation of direct evidence (offset of the MRE horizon) and indirect evidence (FLLS1 deposit) makes a convincing case for earthquake-triggered slides in Fallen Leaf Lake; we extend this logic to the FLLS2. The morphology, source area, and extent of FLLS2 are very similar to FLLS1. Furthermore, FLLS2 is correlated to a significant slide in Lake Tahoe and possibly Emerald Bay and Cascade Lake. Although we lack direct evidence of offset associated with FLLS2, the Tsoyowata Ash horizon appears to diverge slightly toward the southernmost splay of the WTDPF. This splay is at the base of the steeply sloping basin wall, and acoustic artifacts obscure direct imaging of offset horizons. In Emerald Bay, the WTDPF is not imaged due to gas wipeout, but the potentially synchronous slide in Emerald Bay appears to correlate with horizons diverging toward the WTDPF (Fig. 11).

In summary, we infer that FLLS1 and FLLS2 were triggered by an earthquake in the Lake Tahoe Basin for the following reasons. (1) The slides appear to be sourced from the steep slope above the trace of the WTDPF. (2) The observed slide recurrence interval of ~3–4 k.y. is much longer than expected for storm or lake-level fluctuation triggers. (3) The coincident timing of deposits between basins suggests triggering

by a regional, rather than local, event. (4) We observe both direct and indirect earthquake evidence for the MREs on the Fallen Leaf (FLLS1) and Rubicon segments (CLS1) of the WTDPF.

Although the evidence is indirect for FLLS3, we postulate that this slide was also triggered by an earthquake. FLLS3 appears to be synchronous with deposit O in Lake Tahoe and possibly with CLS3 and EBS2 (Table 2; Fig. 15). FLLS3 is smaller than the FLLS1 and FLLS2, but this may reflect the short time period after FLLS4, which could have reset slope stability around the lake. In addition, the slide occurred near the transition from glacial sediments to lacustrine sediments, so we cannot rule out triggering by flooding. FLLS4 is intercalated within glacial sediments and does not appear to be correlated to slides in other subbasins.

We also observe slide CLS1 and deformation along the WTDPF estimated to be ca. 5.2 ka in Cascade Lake. This age estimate is speculative, and therefore it is difficult to confirm temporal correlation between this event and the other basins. However, the MRE on the Rubicon segment of the WTDPF and a slide deposit were dated (Smith et al., 2013) as ca. 5.3–5.6 ka.

These slides could have been triggered by a number of faults in the area, but based on our observations, we believe that the WTDPF is the most likely source. Regionally, the Genoa fault may produce strong shaking in the Lake Tahoe Basin. However, the two most recent events (500–600 yr ago and 2.0–2.2 ka; Ramelli et al., 1999) on the Genoa fault are not associated with major slide events we observed in Fallen Leaf Lake, Emerald Bay, or Cascade Lake. The MRE on the Incline Village fault (500 yr ago; Seitz et al., 2005) also does not appear to have triggered slides in these southern subbasins. The WTDPF is the largest fault in the Lake Tahoe Basin and trends through each of the southern subbasins; therefore, an event on the WTDPF has greater potential to trigger slides than the more distant faults. Furthermore, FLLS1 appears to be synchronous with the MRE on the Fallen Leaf Lake segment of the WTDPF, and CLS1 appears to be synchronous with the MRE on the Rubicon segment of the WTDPF, providing evidence that events on the WTDPF have triggered slides.

Paleoseismic Implications

The slide deposits observed in the subbasins of the Lake Tahoe Basin provide indirect evidence for seismic events as old as ca. 11.5 ka and can be used to calculate a recurrence interval for basin-wide shaking events. The interval between the FLLS1 and FLLS2 event is ~3.1 k.y. and the interval between the FLLS3 event and the FLLS4 event is ~3.7 k.y. Therefore, we cal-

culate a closed recurrence interval for the two slide events in Fallen Leaf Lake of ~3.4 k.y.; if the most recent open interval is included, then a recurrence time of 3.8 k.y. is calculated along the Fallen Leaf segment of the WTDPF. Given that these three slides were likely triggered by earthquakes, one might be tempted to include the ca. 5.3 ka Rubicon event, which reduces the recurrence interval to ~2.9 k.y. for events on the WTDPF, regardless of whether the event was confined to one segment or ruptured across several. In either case, the MRE occurred ca. 4.5 ka, exceeding the calculated recurrence time. In addition to the direct hazard posed by an earthquake in the Lake Tahoe Basin, seismically triggered slides also pose a threat due to the potential to generate tsunamis (Driscoll et al., 2000).

The slide deposits and observed primary deformation also may help constrain rupture patterns in the Lake Tahoe Basin. We observe direct and/or indirect evidence for four potential seismic events in sediments beneath Fallen Leaf Lake, Cascade Lake, Emerald Bay, and Lake Tahoe (Figs. 15 and 16). The MRE on the Fallen Leaf Lake segment of the WTDPF is dated as 4.57–4.85 ka based on the age of coseismic slide deposits (FLLS1). We suggest that deposit F in northern Lake Tahoe, with a modeled age of 4.07–4.51 ka (Smith et al., 2013), was deposited during the same seismic event, which constrains the event age to be ca. 4.5 ka. In Cascade Lake we observe indirect, and potentially direct, evidence of a ca. 5.2 ka event, which may correlate to direct evidence of the MRE on the WTDPF Rubicon segment and associated slide deposit G in Lake Tahoe, dated as ca. 5.3–5.6 ka (Smith et al., 2013). We observe multiple lines of evidence for an event on the WTDPF ca. 8 ka in Lake Tahoe (Smith et al., 2013), Fallen Leaf Lake, and possibly Emerald Bay and Cascade Lake. We observe only secondary evidence for an event ca. 11.5 ka; this event is represented by slides in Lake Tahoe (Smith et al., 2013) and Fallen Leaf Lake, and possibly Emerald Bay and Cascade Lake.

The geographic distribution of slides illustrated in Figure 16 may suggest that the entire basin underwent shaking ca. 11.5 ka and ca. 8 ka, which might be due to a full rupture along all three segments of the WTDPF. The younger events, however, may reflect segmented rupture. The ca. 5.3–5.6 ka event on the Rubicon segment may have only ruptured the northern and central segments of the WTDPF, whereas a ca. 4.57–4.85 ka event may have ruptured only the Fallen Leaf Lake segment of the WTDPF. Nevertheless, the alternative also needs to be considered; that is, rupture of even one segment of the WTDPF might generate

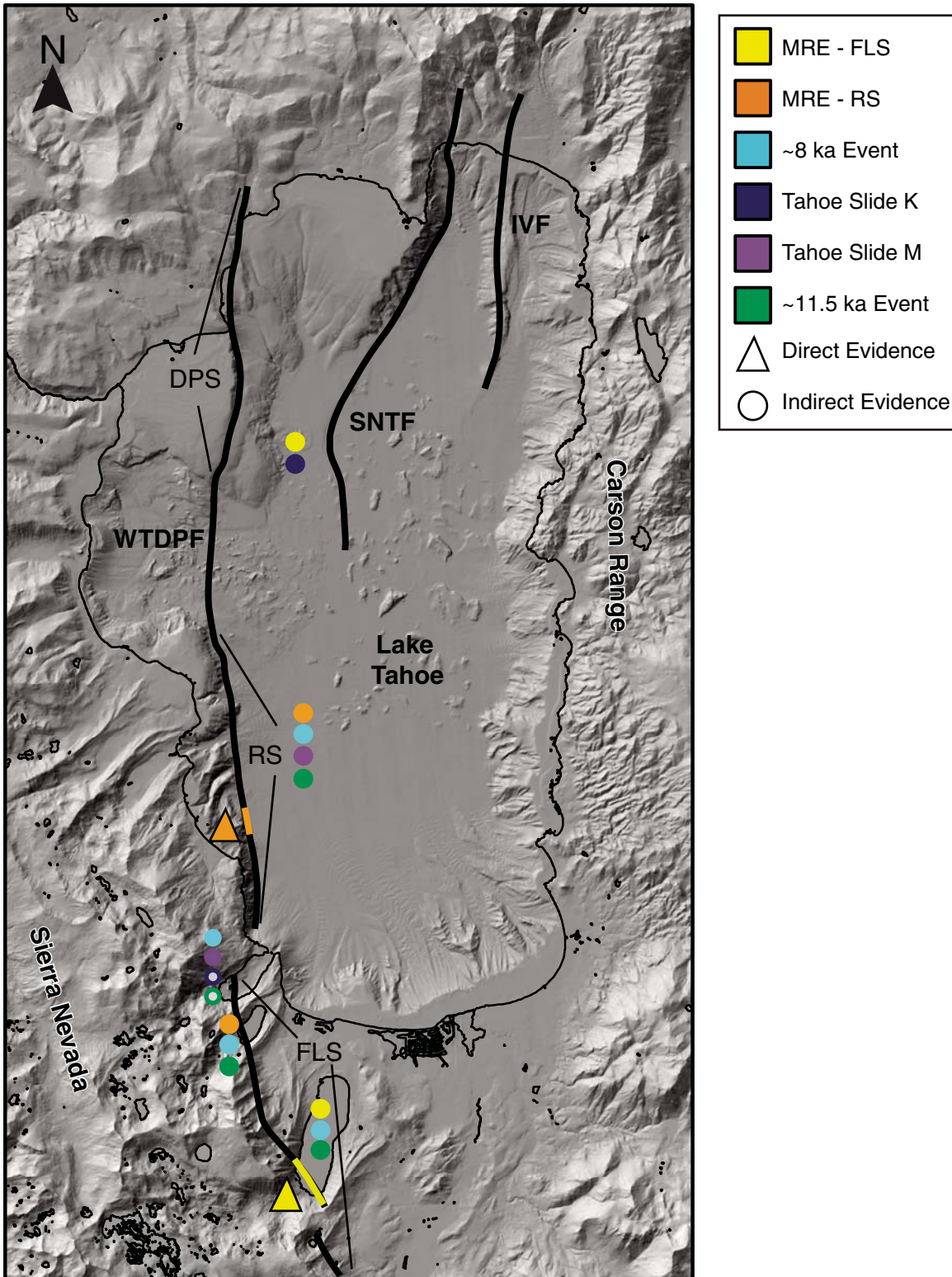


Figure 16. Map of the Lake Tahoe Basin showing direct and indirect evidence of seismic events in the four sub-basins (Lake Tahoe, Fallen Leaf Lake, Emerald Bay, and Cascade Lake). Circles represent slide deposits, colored by their approximate ages. The trace of the West Tahoe–Dollar Point fault (WTDPF) is colored by event age (see legend) and marked with a triangle where direct evidence of faulting is observed. MRE—most recent event; DPS—Dollar Point segment; IVF—Incline Village fault; SNTF—Stateline–North Tahoe fault; FLS—Fallen Leaf segment; RS—Rubicon segment.

Paleoseismic history of the Fallen Leaf segment of the West Tahoe–Dollar Point fault

sufficient ground motion to trigger failures basin wide. For example, the MRE on the Fallen Leaf Lake segment of the WTDPF might have triggered a slide as far away as the northern part of Lake Tahoe. Additional work is warranted to understand how the segments of the WTDPF accommodate deformation, whether they rupture in concert or alone.

Recent studies of Lidar data and offset moraines suggest that the Fallen Leaf Lake segment of the WTDPF identified in Chirp and Lidar data is equivalent to the Mount Tallac segment of the purported Tahoe–Sierra frontal fault zone (Howle et al., 2012). Difficulties arise with this interpretation, based on both fault architecture and recurrence interval. Our preferred option is that this fault is the southernmost segment of the WTDPF system and the determined fault recurrence interval reported here is more consistent with lower vertical slip rates reported for the WTDPF (0.4–0.8 mm/yr) than the two-fold to threefold increase in slip rate reported for the Tahoe–Sierra frontal fault zone (1.1–1.9 mm/yr; Howle et al., 2012). We have mapped the Fallen Leaf Lake segment of the WTDPF in Chirp and Lidar extending from southern Fallen Leaf Lake to Cascade Lake. Diverging beds in Emerald Bay also suggest that this segment may continue and die into Emerald Bay in a number of splays (e.g., Fig. 9). The Rubicon segment of the WTDPF is mapped along the steep western slope from just north of Emerald Bay to McKinney Bay (Fig. 1). The ~2 km step between the Fallen Leaf Lake segment and Rubicon segment is well within the range documented by previous studies (3–4 km; Wesnousky, 2006) for rupture propagation across a stepover.

CONCLUSIONS

Coincident slides in Fallen Leaf Lake, Lake Tahoe, and perhaps Cascade Lake and Emerald Bay support earthquake shaking as the most plausible triggering mechanism. The geographic distribution of the slide events and direct offset evidence further suggests that the segments of the WTDPF may sometimes rupture in concert and other times individually. The recurrence time for events on the Fallen Leaf segment of the WTDPF is ~3–4 k.y., and the time since the MRE (ca. 4.5 ka) exceeds the calculated recurrence time.

Much of our understanding of segment interactions is based on surficial measurements (i.e., Lidar and trenching). The data presented here provide information about earthquake recurrence and how segments interact through longer time intervals. Such data sets combined with surficial measurements will provide an improved understanding of what controls

whether ruptures propagate from one segment to another.

ACKNOWLEDGMENTS

This research was supported by National Science Foundation grants OCE-0649410 and EAR-127499, U.S. Geological Survey National Earthquake Hazards Reduction Program grants 10HQPA1000, 06HQGR0064, and 02HQGR0072, and an Exxon-Mobil student grant. This manuscript was greatly enhanced through thoughtful reviews from Cathy Busby, Paul Umhoefer, Mike Oskin, and Rich Briggs. Radiocarbon ages for the 2010 Fallen Leaf Lake cores were funded by Lawrence Livermore National Laboratory Laboratory Directed Research and Development grant 09-ERI-003. We thank Brig Ebrigh for his permission to allow us to conduct research on Cascade Lake and Paul Baker for access to a boat ramp on his property. We are indebted to Fire Chief Gary Gerren for access to the Fallen Leaf Lake boat ramp and invasive species boat wash. Generous support from Bill Craven and access to his boat allowed collection of the 2010 multibeam survey. We also thank Shane Romsos and the Tahoe Regional Planning Agency for access to the critical airborne Lidar (light detection and ranging) data collected in 2010. We thank Anders Noren and Kristina Brady from LacCore for adding Fallen Leaf Lake to their busy 2010 coring schedule and for helping us get a high-quality suite of piston cores. Initial core processing, logging, and sampling of the 2010 Fallen Leaf Lake cores were conducted at LacCore. We thank Laurel Stratton for her logistical role in initiating the 2010 coring program and for helping with initial core processing, and Danny Brothers for conversations regarding previously collected Chirp (compressed high intensity radar pulse) profiles and sediment cores.

REFERENCES CITED

- Argus, D.F., and Gordon, R.G., 2001, Present tectonic motion across the Coast Ranges and San Andreas fault system in central California: *Geological Society of America Bulletin*, v. 113, p. 1580–1592, doi:10.1130/0016-7606(2001)113<1580:PTMATC>2.0.CO;2.
- Bacon, C.R., 1983, Eruptive history of Mount Mazama and Crater Lake Caldera, Cascade Range, USA: *Journal of Volcanology and Geothermal Research*, v. 18, p. 57–115, doi:10.1016/0377-0273(83)90004-5.
- Bennett, R.A., Wernicke, B.P., Niemi, N.A., Friedrich, A.M., and Davis, J.L., 2003, Contemporary strain rates in the northern Basin and Range Province from GPS data: *Tectonics*, v. 22, doi:10.1029/2001TC001355.
- Benson, L., Kashgarian, M., Rye, R.O., Lund, S.P., Paillet, F.L., Smoot, J.P., Kester, C.L., Mensing, S., Meko, D., and Lindstrom, S., 2002, Holocene multidecadal and multicentennial droughts affecting northern California and Nevada: *Quaternary Science Reviews*, v. 21, p. 659–682, doi:10.1016/S0277-3791(01)00048-8.
- Benson, L.V., May, H.M., Antweiler, R.C., Brinton, T.L., Kashgarian, M., Smoot, J.P., and Lund, S.P., 1998, Continuous lake-sediment records of glaciation in the Sierra Nevada between 52,600 and 12,500 radiocarbon yrs B.P.: *Quaternary Research*, v. 50, p. 113–127, doi:10.1006/qres.1998.1993.
- Bischoff, J.L., and Cummins, K., 2001, Wisconsin Glaciation of the Sierra Nevada (79,000–15,000 yr B.P.) as recorded by rock flour in sediments of Owens Lake, California: *Quaternary Research*, v. 55, p. 14–24, doi:10.1006/qres.2000.2183.
- Bronk Ramsey, C., 2009, Bayesian analysis of radiocarbon dates: *Radiocarbon*, v. 51, p. 337–360.
- Brothers, D.S., Kent, G.M., Driscoll, N.W., Smith, S.B., Karlin, R., Dingler, J.A., Harding, A.J., Seitz, G.G., and Babcock, J.M., 2009, New constraints on deformation,

- slip rate, and timing of the most recent earthquake on the West Tahoe–Dollar Point fault, Lake Tahoe Basin, California: *Seismological Society of America Bulletin*, v. 99, p. 499–519, doi:10.1785/0120080135.
- Clark, D.H., and Gillespie, A.R., 1997, Timing and significance of late-glacial and Holocene cirque glaciation in the Sierra Nevada, California: *Quaternary International*, v. 38/39, p. 21–38, doi:10.1016/S1040-6182(96)00024-9.
- Dingler, J., Kent, G., Driscoll, N., Babcock, J., Harding, A., Seitz, G., Karlin, B., and Goldman, C., 2009, A high-resolution seismic CHIRP investigation of active normal faulting across Lake Tahoe basin, California–Nevada: *Geological Society of America Bulletin*, v. 121, p. 1089–1107, doi:10.1130/B26244.1.
- Dixon, T.H., Miller, M., Farina, F., Wang, H., and Johnson, D., 2000, Present-day motion of the Sierra Nevada block and some tectonic implications for the Basin and Range Province, North American Cordillera: *Tectonics*, v. 19, p. 1–24, doi:10.1029/1998TC001088.
- Driscoll, N.W., Weissel, J.K., and Goff, J.A., 2000, Potential for large-scale submarine slope failure and tsunami generation along the U.S. mid-Atlantic coast: *Geology*, v. 28, p. 407–410, doi:10.1130/0091-7613(2000)28<407:PFLSSF>2.0.CO;2.
- Faulds, J.E., Henry, C.D., and Hinz, N.H., 2005, Kinematics of the northern Walker Lane: An incipient transform fault along the Pacific–North American plate boundary: *Geology*, v. 33, p. 505–508, doi:10.1130/G21274.1.
- Gardner, J.V., Mayer, L.A., and Hughs Clarke, J.E., 2000, Morphology and processes in Lake Tahoe (California–Nevada): *Geological Society of America Bulletin*, v. 112, p. 736–746, doi:10.1130/0016-7606(2000)112<736:MAPILT>2.0.CO;2.
- Goldfinger, C., Morey, A.E., Nelson, C.H., Gutierrez-Pastor, J., Johnson, J.E., Karabanov, E., Chaytor, J., Eriksson, A., and Party, S.S., 2007, Rupture lengths and temporal history of significant earthquakes on the offshore and north coast segments of the northern San Andreas fault based on turbidite stratigraphy: *Earth and Planetary Science Letters*, v. 254, p. 9–27, doi:10.1016/j.epsl.2006.11.017.
- Hammond, W.C., and Thatcher, W., 2004, Contemporary tectonic deformation of the Basin and Range Province, western United States; 10 years of observation with the Global Positioning System: *Journal of Geophysical Research*, v. 109, no. B8, doi:10.1029/2003JB002746.
- Hampton, M.A., Lee, H.J., and Locat, J., 1996, Submarine landslides: *Reviews of Geophysics*, v. 34, p. 33–59, doi:10.1029/95RG03287.
- Henkart, P., 2003, SIOSEIS software: La Jolla, California, Scripps Institution of Oceanography, <http://sioseis.ucsd.edu>.
- Howle, J.F., Bawden, G.W., Schweickert, R.A., Finkel, R.C., Hunter, L.E., Rose, R.S., and von Twisting, B., 2012, Airborne LiDAR analysis and geochronology of faulted glacial moraines in the Tahoe–Sierra frontal fault zone reveal substantial seismic hazards in the Lake Tahoe region, California–Nevada, USA: *Geological Society of America Bulletin*, v. 124, p. 1087–1101, doi:10.1130/B30598.1.
- Hynes, N.J., Chelminski, P., Court, J.E., Gorsline, D.S., and Goldman, C.R., 1972, Quaternary history of Lake Tahoe, California–Nevada: *Geological Society of America Bulletin*, v. 83, p. 1435–1448, doi:10.1130/0016-7606(1972)83<1435:QHOLTJ>2.0.CO;2.
- Karlin, R., Noble, P.J., Zimmerman, S.H., Stratton, L., Smith, S.B., Kent, G., Maloney, J., and Driscoll, N.W., 2011, BOLLY Project—Preliminary multi-proxy data from Holocene cores, Fallen Leaf Lake, Tahoe Basin, California, USA: *Geological Society of America Abstracts with Programs*, v. 43, no. 5, p. 468.
- Karlin, R.E., Smith, S., Seitz, G.G., Kent, G.M., and Driscoll, N.W., 2005, Landslides, active faulting, and paleoseismicity in Lake Tahoe: *Seismological Research Letters*, v. 76, p. 250.
- Kent, G.M., and 14 others, 2005, 60 k.y. record of extension across the western boundary of the Basin and Range province: Estimate of slip rates from offset shoreline terraces and a catastrophic slide beneath Lake Tahoe: *Geology*, v. 33, p. 365–368, doi:10.1130/G21230.1.

- Kleppe, J.A., Brothers, D.S., Kent, G.M., Biondi, F., Jensen, S., and Driscoll, N.W., 2011, Duration and severity of Medieval drought in the Lake Tahoe Basin: Quaternary Science Reviews, v. 30, p. 3269–3279, doi:10.1016/j.quascirev.2011.08.015.
- Lee, H.J., Greene, H.G., Edwards, B.D., Fisher, M.A., and Normark, W.R., 2009, Submarine landslides of the Southern California Borderland, in Lee, H.J., and Normark, W.R., eds., Earth science in the urban ocean: The Southern California Continental Borderland: Geological Society of America Special Paper 454, p. 251–269, doi:10.1130/2009.2454(4.3).
- Oldow, J.S., 2003, Active transtensional boundary zone between the western Great Basin and Sierra Nevada block, western U.S. Cordillera: Geology, v. 31, p. 1033–1036, doi:10.1130/G19838.1.
- Phillips, F.M., Zreda, M.G., Benson, L.V., Plummer, M.A., Elmore, D., and Sharma, P., 1996, Chronology for fluctuations in late Pleistocene Sierra Nevada glaciers and lakes: Science, v. 274, no. 5288, p. 749–751, doi:10.1126/science.274.5288.749.
- Ramelli, A.R., Bell, J.W., dePolo, C.M., and Yount, J.C., 1999, Large-magnitude late Holocene earthquakes on the Genoa fault, west-central Nevada and eastern California: Seismological Society of America Bulletin, v. 89, p. 1458–1472.
- Reimer, P.J., and 28 others, 2004, IntCal04 terrestrial radiocarbon age calibration, 0–26 cal kyr BP: Radiocarbon, v. 46, p. 1029–1058.
- Rood, D.H., Burbank, D.W., and Finkel, R.C., 2011, Chronology of glaciations in the Sierra Nevada, California, from ¹⁰Be surface exposure dating: Quaternary Science Reviews, v. 30, p. 646–661, doi:10.1016/j.quascirev.2010.12.001.
- Sarna-Wojcicki, A.M., Lajoie, K.R., Meyer, C.E., Adam, D.P., and Rieck, H.J., 1991, Tephrochronology correlation of upper Neogene sediments along the Pacific margin, conterminous United States, in Morrison, R.B., ed., Quaternary nonglacial geology: Conterminous United States: Boulder, Colorado, Geological Society of America, Geology of North America, v. K-2, p. 117–140.
- Saucedo, G.J., Little, J.D., Watkins, S.E., Davis, J.R., Mascorro, M.T., Walker, V.D., and Ford, E.W., 2005, Geologic map of the Lake Tahoe Basin, California and Nevada: California Geological Survey Regional Geologic Map no. 4, scale 1:100,000.
- Schnellmann, M., Anselmetti, F.S., Giardini, D., McKenzie, J.A., and Ward, S.N., 2002, Prehistoric earthquake history revealed by lacustrine slump deposits: Geology, v. 30, p. 1131–1134, doi:10.1130/0091-7613(2002)030<1131:PEHRBL>2.0.CO;2.
- Schweickert, R.A., Lahren, M.M., Smith, K.D., Howle, J.F., and Ichinose, G.A., 2004, Transtensional deformation in the Lake Tahoe region, California and Nevada, USA: Tectonophysics, v. 392, p. 303–323, doi:10.1016/j.tecto.2004.04.019.
- Seitz, G.G., Kent, G.M., Dingler, J.A., Karlin, B., and Turner, R., 2005, First paleoseismic results from the Lake Tahoe basin; evidence for three M 7 range earthquakes on the Incline Village fault: Seismological Research Letters, v. 76, p. 239–240.
- Seitz, G., Kent, G., Smith, S., Dingler, J., Driscoll, N., Karlin, R., Babcock, J., and Harding, A., 2006, Multi-method paleoseismology; combining on and offshore data to build a basin wide record of earthquakes at Lake Tahoe: Seismological Research Letters, v. 77, p. 274.
- Smith, S.B., Karlin, R.E., Kent, G., Seitz, G., and Driscoll, N.W., 2013, Holocene subaqueous paleoseismology of Lake Tahoe: Geological Society of America Bulletin, v. 125, p. 691–708, doi:10.1130/B30629.1.
- Strasser, M., Anselmetti, F.S., Faeh, D., Giardini, D., and Schnellmann, M., 2006, Magnitudes and source areas of large prehistoric northern Alpine earthquakes revealed by slope failures in lakes: Geology, v. 34, p. 1005–1008, doi:10.1130/G22784A.1.
- Stuiver, M., and Polach, H.A., 1977, Discussion; reporting of ¹⁴C data: Radiocarbon, v. 19, p. 355–363.
- Surpless, B.E., Stockli, D.F., Dumitru, T.A., and Miller, E.L., 2002, Two-phase westward encroachment of Basin and Range extension into the northern Sierra Nevada: Tectonics, v. 21, p. 2–1–2–10, doi:10.1029/2000TC001257.
- Svarc, J.L., Savage, J.C., Prescott, W.H., and Ramelli, A.R., 2002, Strain accumulation and rotation in western Nevada, 1993–2000: Journal of Geophysical Research, v. 107, no. B5, p. ETG 2–1–ETG 2–11, doi:10.1029/2001JB000579.
- Tahoe Regional Planning Agency, 2010, Lake Tahoe Basin LiDAR: <http://dx.doi.org/10.5069/G9PN93H2> (October 2011).
- Uchupi, E., and Ross, D.A., 2000, Early Holocene marine flooding of the Black Sea: Quaternary Research, v. 54, p. 68–71, doi:10.1006/qres.2000.2149.
- Unruh, J., Humphrey, J., and Barron, A., 2003, Transtensional model for the Sierra Nevada frontal fault system, eastern California: Geology, v. 31, p. 327–330, doi:10.1130/0091-7613(2003)031<0327:TMFTSN>2.0.CO;2.
- Upton, P., and Osterberg, E.C., 2007, Paleoseismicity and mass movements interpreted from seismic-reflection data, Lake Tekapo, South Canterbury, New Zealand: New Zealand Journal of Geology and Geophysics, v. 50, p. 343–356, doi:10.1080/00288300709509841.
- U.S. Geological Survey, Coastal and Marine Geology (CMG), Chief Scientist James V. Gardner, 2001, Multibeam mapping of Lake Tahoe, California-Nevada from field activity: L-1–98-LT: http://tahoe.usgs.gov/bath_download.html (October 2011).
- Wesnousky, S.G., 2006, Predicting the endpoints of earthquake ruptures: Nature, v. 444, p. 358–360, doi:10.1038/nature05275.